A Theory for Multiresolution Signal Decomposition: The Wavelet Representation

STEPHANE G. MALLAT

Abstract—Multiresolution representations are very effective for analyzing the information content of images. We study the properties of the operator which approximates a signal at a given resolution. We show that the difference of information between the approximation of a signal at the resolutions 2^{j+1} and 2^j can be extracted by decomposing this signal on a wavelet orthonormal basis of $L^2(R^n)$. In $L^2(R)$, a wavelet orthonormal basis is a family of functions $(\sqrt{2^j}\, \psi(2^j x - n))_{(j,n)\in Z^2}$, which is built by dilating and translating a unique function $\psi(x)$. This decomposition defines an orthogonal multiresolution representation called a wavelet representation. It is computed with a pyramidal algorithm based on convolutions with quadrature mirror filters. For images, the wavelet representation differentiates several spatial orientations. We study the application of this representation to data compression in image coding, texture discrimination and fractal analysis.

Index Terms—Coding, fractals, multiresolution pyramids, quadrature mirror filters, texture discrimination, wavelet transform.

I. INTRODUCTION

IN computer vision, it is difficult to analyze the information content of an image directly from the gray-level intensity of the image pixels. Indeed, this value depends upon the lighting conditions. More important are the local variations of the image intensity. The size of the neighborhood where the contrast is computed must be adapted to the size of the objects that we want to analyze [41]. This size defines a resolution of reference for measuring the local variations of the image. Generally, the structures we want to recognize have very different sizes. Hence, it is not possible to define a priori an optimal resolution for analyzing images. Several researchers [18], [31], [42] have developed pattern matching algorithms which process the image at different resolutions. For this purpose, one can reorganize the image information into a set of details appearing at different resolutions. Given a sequence of increasing resolutions $(r_j)_{j \in Z}$, the details of an image at the resolution r_j are defined as the difference of information between its approximation at the resolution r_j and its approximation at the lower resolution r_{j-1}.

A multiresolution decomposition enables us to have a scale-invariant interpretation of the image. The scale of an image varies with the distance between the scene and the optical center of the camera. When the image scale is modified, our interpretation of the scene should not change. A multiresolution representation can be partially scale-invariant if the sequence of resolution parameters $(r_j)_{j \in Z}$ varies exponentially. Let us suppose that there exists a resolution step $\alpha \in R$ such that for all integers j, $r_j = \alpha^j$. If the camera gets α times closer to the scene, each object of the scene is projected on an area α^2 times bigger in the focal plane of the camera. That is, each object is measured at a resolution α times bigger. Hence, the details of this new image at the resolution α^j correspond to the details of the previous image at the resolution α^{j+1}. Rescaling the image by α translates the image details along the resolution axis. If the image details are processed identically at all resolutions, our interpretation of the image information is not modified.

A multiresolution representation provides a simple hierarchical framework for interpretating the image information [22]. At different resolutions, the details of an image generally characterize different physical structures of the scene. At a coarse resolution, these details correspond to the larger structures which provide the image "context". It is therefore natural to analyze first the image details at a coarse resolution and then gradually increase the resolution. Such a coarse-to-fine strategy is useful for pattern recognition algorithms. It has already been widely studied for low-level image processing such as stereo matching and template matching [16], [18].

Burt [5] and Crowley [8] have each introduced pyramidal implementation for computing the signal details at different resolutions. In order to simplify the computations, Burt has chosen a resolution step α equal to 2. The details at each resolution 2^j are calculated by filtering the original image with the difference of two low-pass filters and by subsampling the resulting image by a factor 2^j. This operation is performed over a finite range of resolutions. In this implementation, the difference of low-pass filters gives an approximation of the Laplacian of the Gaussian. The details at different resolutions are regrouped into a pyramid structure called the Laplacian pyramid. The Laplacian pyramid data structures, as studied by Burt and Crowley, suffer from the difficulty that data at separate levels are correlated. There is no clear model

which handles this correlation. It is thus difficult to know whether a similarity between the image details at different resolutions is due to a property of the image itself or to the intrinsic redundancy of the representation. Furthermore, the Laplacian multiresolution representation does not introduce any spatial orientation selectivity into the decomposition process. This spatial homogeneity can be inconvenient for pattern recognition problems such as texture discrimination [21].

In this article, we first study the mathematical properties of the operator which transforms a function into an approximation at a resolution 2^j. We then show that the difference of information between two approximations at the resolutions 2^{j+1} and 2^j is extracted by decomposing the function in a wavelet orthonormal basis. This decomposition defines a complete and orthogonal multiresolution representation called the wavelet representation. Wavelets have been introduced by Grossmann and Morlet [17] as functions $\psi(x)$ whose translations and dilations $(\sqrt{s}\,\psi(sx - t))_{(s,t)\in R^+ \times R}$ can be used for expansions of $L^2(R)$ functions. Meyer [35] showed that there exists wavelets $\psi(x)$ such that $(\sqrt{2^j}\,\psi(2^j x - k))_{(j,k)\in Z^2}$ is an orthonormal basis of $L^2(R)$. These bases generalize the Haar basis. The wavelet orthonormal bases provide an important new tool in functional analysis. Indeed, before then, it had been believed that no construction could yield simple orthonormal bases of $L^2(R)$ whose elements had good localization properties in both the spatial and Fourier domains.

The multiresolution approach to wavelets enables us to characterize the class of functions $\psi(x) \in L^2(R)$ that generate an orthonormal basis. The model is first described for one-dimensional signals and then extended to two dimensions for image processing. The wavelet representation of images discriminates several spatial orientations. We show that the computation of the wavelet representation may be accomplished with a pyramidal algorithm based on convolutions with quadrature mirror filters. The signal can also be reconstructed from a wavelet representation with a similar pyramidal algorithm. We discuss the application of this representation to compact image coding, texture discrimination and fractal analysis. In this article, we omit the proofs of the theorems and avoid mathematical technical details. Rather, we try to illustrate the practical implications of the model. The mathematical foundations are more thoroughly described in [28].

A. Notation

Z and **R** denote the set of integers and real numbers respectively. $L^2(R)$ denotes the vector space of measurable, square-integrable one-dimensional functions $f(x)$. For $f(x) \in L^2(R)$ and $g(x) \in L^2(R)$, the inner product of $f(x)$ with $g(x)$ is written

$$\langle g(u), f(u) \rangle = \int_{-\infty}^{+\infty} g(u) f(u)\, du.$$

The norm of $f(x)$ in $L^2(R)$ is given by

$$\|f\|^2 = \int_{-\infty}^{+\infty} |f(u)|^2\, du.$$

We denote the convolution of two functions $f(x) \in L^2(R)$ and $g(x) \in L^2(R)$ by

$$f * g(x) = (f(u) * g(u))(x)$$

$$= \int_{-\infty}^{+\infty} f(u)\, g(x - u)\, du.$$

The Fourier transform of $f(x) \in L^2(R)$ is written $\hat{f}(\omega)$ and is defined by

$$\hat{f}(\omega) = \int_{-\infty}^{+\infty} f(x)\, e^{-i\omega x}\, dx.$$

$I^2(Z)$ is the vector space of square-summable sequences

$$I^2(Z) = \left\{ (\alpha_i)_{i\in Z} : \sum_{i=-\infty}^{+\infty} |\alpha_i|^2 < \infty \right\}.$$

$L^2(R^2)$ is the vector space of measurable, square-integrable two dimensional functions $f(x, y)$. For $f(x, y) \in L^2(R^2)$ and $g(x, y) \in L^2(R^2)$, the inner product of $f(x, y)$ with $g(x, y)$ is written

$$\langle f(x, y), g(x, y) \rangle = \int_{-\infty}^{+\infty} \int_{-\infty}^{+\infty} f(x, y)\, g(x, y)\, dx\, dy.$$

The Fourier transform of $f(x, y) \in L^2(R^2)$ is written $\hat{f}(\omega_x, \omega_y)$ and is defined by

$$\hat{f}(\omega_x, \omega_y) = \int_{-\infty}^{+\infty} \int_{-\infty}^{+\infty} f(x, y)\, e^{-i(\omega_x x + \omega_y y)}\, dx\, dy.$$

II. MULTIRESOLUTION TRANSFORM

In this section, we study the concept of multiresolution decomposition for one-dimensional signals. The model is extended to two dimensions in Section IV.

A. Multiresolution Approximation of $L^2(R)$

Let A_{2^j} be the operator which approximates a signal at a resolution 2^j. We suppose that our original signal $f(x)$ is measurable and has a finite energy: $f(x) \in L^2(R)$. Here, we characterize A_{2^j} from the intuitive properties that one would expect from such an approximation operator. We state each property in words, and then give the equivalent mathematical formulation.

1) A_{2^j} is a linear operator. If $A_{2^j} f(x)$ is the approximation of some function $f(x)$ at the resolution 2^j, then $A_{2^j} f(x)$ is not modified if we approximate it again at the resolution 2^j. This principle shows that $A_{2^j} \circ A_{2^j} = A_{2^j}$. The operator A_{2^j} is thus a projection operator on a particular vector space $V_{2^j} \subset L^2(R)$. The vector space V_{2^j} can be interpreted as the set of all possible approximations at the resolution 2^j of functions in $L^2(R)$.

2) Among all the approximated functions at the resolution 2^j, $A_{2^j} f(x)$ is the function which is the most similiar to $f(x)$.

$$\forall g(x) \in V_{2^j}, \quad \|g(x) - f(x)\| \geq \|A_{2^j}f(x) - f(x)\|.$$
$$(1)$$

Hence, the operator A_{2^j} is an orthogonal projection on the vector space V_{2^j}.

3) The approximation of a signal at a resolution 2^{j+1} contains all the necessary information to compute the same signal at a smaller resolution 2^j. This is a causality property. Since A_{2^j} is a projection operator on V_{2^j} this principle is equivalent to

$$\forall j \in Z, \quad V_{2^j} \subset V_{2^{j+1}}. \qquad (2)$$

4) An approximation operation is similar at all resolutions. The spaces of approximated functions should thus be derived from one another by scaling each approximated function by the ratio of their resolution values

$$\forall j \in Z, \quad f(x) \in V_{2^j} \Leftrightarrow f(2x) \in V_{2^{j+1}}. \qquad (3)$$

5) The approximation $A_{2^j}f(x)$ of a signal $f(x)$ can be characterized by 2^j samples per length unit. When $f(x)$ is translated by a length proportional to 2^{-j}, $A_{2^j}f(x)$ is translated by the same amount and is characterized by the same samples which have been translated. As a consequence of (3), it is sufficient to express the principle 5) for the resolution $j = 0$. The mathematical translations consist of the following.

• Discrete characterization:

There exists an isomorphism I from V_1 onto $l^2(Z)$.
$$(4)$$

• Translation of the approximation:

$$\forall k \in Z, A_1 f_k(x)$$
$$= A_1 f(x - k), \text{ where } f_k(x) = f(x - k). \quad (5)$$

• Translation of the samples:

$$I(A_1 f(x)) = (\alpha_i)_{i \in Z} \Leftrightarrow I(A_1 f_k(x)) = (\alpha_{i-k})_{i \in Z}. \quad (6)$$

6) When computing an approximation of $f(x)$ at resolution 2^j, some information about $f(x)$ is lost. However, as the resolution increases to $+\infty$ the approximated signal should converge to the original signal. Conversely as the resolution decreases to zero, the approximated signal contains less and less information and converges to zero.

Since the approximated signal at a resolution 2^j is equal to the orthogonal projection on a space V_{2^j}, this principle can be written

$$\lim_{j \to +\infty} V_{2^j} = \bigcup_{j=-\infty}^{+\infty} V_{2^j} \text{ is dense in } L^2(R) \qquad (7)$$

and

$$\lim_{j \to -\infty} V_{2^j} = \bigcap_{j=-\infty}^{+\infty} V_{2^j} = \{0\}. \qquad (8)$$

We call any set of vector spaces $(V_{2^j})_{j \in Z}$ which satisfies the properties (2)–(8) a *multiresolution approximation* of $L^2(R)$. The associated set of operators A_{2^j} satisfying 1)–6) give the approximation of any $L^2(R)$ function at a res-

olution 2^j. We now give a simple example of a multiresolution approximation of $L^2(R)$.

Example: Let V_1 be the vector space of all functions of $L^2(R)$ which are constant on each interval $]k, k+1[$, for any $k \in Z$. Equation (3) implies that V_{2^j} is the vector space of all the functions of $L^2(R)$ which are constant on each interval $]k2^{-j}, (k+1)2^{-j}[$, for any $k \in Z$. The condition (2) is easily verified. We can define an isomorphism I which satisfies properties (4), (5), and (6) by associating with any function $f(x) \in V_1$ the sequence $(\alpha_k)_{k \in Z}$ such that α_k equals the value of $f(x)$ on the interval $]k, k+1[$. We know that the vector space of piecewise constant functions is dense in $L^2(R)$. Hence, we can derive that $\bigcup_{j=-\infty}^{+\infty} V_{2^j}$ is dense in $L^2(R)$. It is clear that $\bigcap_{j=-\infty}^{+\infty} V_{2^j} = \{0\}$, so the sequence of vector spaces $(V_{2^j})_{j \in Z}$ is a multiresolution approximation of $L^2(R)$. Unfortunately, the functions of these vector spaces are neither smooth nor continuous, making this multiresolution approximation rather inconvenient. For many applications we want to compute a smooth approximation. In Appendix A, we describe a class of multiresolution approximations where the functions of each space V_{2^j} are n times continuously differentiable.

We saw that the approximation operator A_{2^j} is an orthogonal projection on the vector space V_{2^j}. In order to numerically characterize this operator, we must find an orthonormal basis of V_{2^j}. The following theorem shows that such an orthonormal basis can be defined by dilating and translating a unique function $\phi(x)$.

Theorem 1: Let $(V_{2^j})_{j \in Z}$ be a multiresolution approximation of $L^2(R)$. There exists a unique function $\phi(x) \in L^2(R)$, called a *scaling function*, such that if we set $\phi_{2^j}(x) = 2^j \phi(2^j x)$ for $j \in Z$, (the dilation of $\phi(x)$ by 2^j), then

$$\left(\sqrt{2^{-j}} \phi_{2^j}(x - 2^{-j}n)\right)_{n \in Z} \text{ is an orthonormal basis of } V_{2^j}.$$

■ (9)

Indications for the proof of this theorem can be found in Appendix B. The theorem shows that we can build an orthonormal basis of any V_{2^j} by dilating a function $\phi(x)$ with a coefficient 2^j and translating the resulting function on a grid whose interval is proportional to 2^{-j}. The functions $\phi_{2^j}(x)$ are normalized with respect to the $L^1(R)$ norm. The coefficient $\sqrt{2^{-j}}$ appears in the basis set in order to normalize the functions in the $L^2(R)$ norm. For a given multiresolution approximation $(V_{2^j})_{j \in Z}$, there exists a unique scaling function $\phi(x)$ which satisfies (9). However, for different multiresolution approximations, the scaling functions are different. One can easily show that the scaling function corresponding to the multiresolution described in the previous example is the indicator function of the interval $[0, 1]$. In general, we want to have a smoother scaling function. Fig. 1 shows an example of a continuously differentiable and exponentially decreasing scaling function. Its Fourier transform has the shape of a
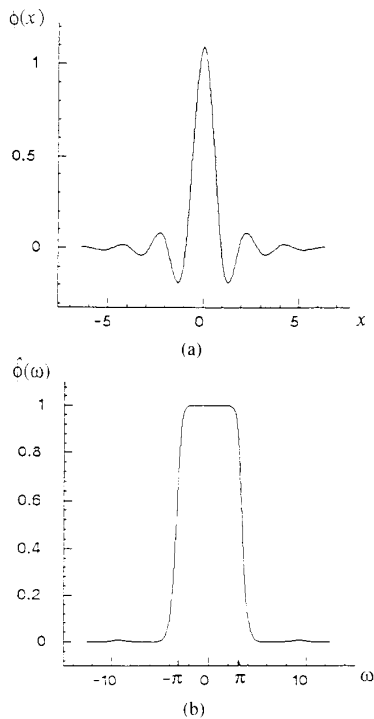
Fig. 1. (a) Example of scaling function $\phi(x)$. This function is computed in Appendix A. (b) Fourier transform $\hat{\phi}(\omega)$. A scaling function is a low-pass filter.

low-pass filter. The corresponding multiresolution approximation is built from cubic splines. This scaling function is described further in Appendix A.

The orthogonal projection on V_{2^j} can now be computed by decomposing the signal $f(x)$ on the orthonormal basis given by Theorem 1. Specifically,

$$\forall f(x) \in L^2(R), \ A_{2^j} f(x)$$
$$= 2^{-j} \sum_{n=-\infty}^{+\infty} \langle f(u), \phi_{2^j}(u - 2^{-j}n) \rangle \ \phi_{2^j}(x - 2^{-j}n).$$
$$(10)$$

The approximation of the signal $f(x)$ at the resolution 2^j, $A_{2^j} f(x)$, is thus characterized by the set of inner products which we denote by

$$A_{2^j}^d f = \left(\langle f(u), \phi_{2^j}(u - 2^{-j}n) \rangle \right)_{n \in Z}. \quad (11)$$

$A_{2^j}^d f$ is called a *discrete approximation* of $f(x)$ at the resolution 2^j. Since computers can only process discrete signals, we must work with discrete approximations. Each inner product can also be interpreted as a convolution product evaluated at a point $2^{-j}n$

$$\langle f(u), \phi_{2^j}(u - 2^{-j}n) \rangle$$
$$= \int_{-\infty}^{+\infty} f(u) \ \phi_{2^j}(u - 2^{-j}n) \ du$$
$$= \left(f(u) * \phi_{2^j}(-u) \right)(2^{-j}n).$$

Hence, we can rewrite $A_{2^j}^d f$:

$$A_{2^j}^d f = \left(\left(f(u) * \phi_{2^j}(-u) \right)(2^{-j}n) \right)_{n \in Z}. \quad (12)$$

Since $\phi(x)$ is a low-pass filter, this discrete signal can be interpreted as a low-pass filtering of $f(x)$ followed by a uniform sampling at the rate 2^j. In an approximation operation, when removing the details of $f(x)$ smaller than 2^{-j}, we suppress the highest frequencies of this function. The scaling function $\phi(x)$ forms a very particular low-pass filter since the family of functions $(\sqrt{2^{-j}} \ \phi_{2^j}(x - 2^{-j}n))_{n \in Z}$ is an orthonormal family.

In the next section we show that the discrete approximation of $f(x)$ at the resolution 2^j can be computed with a pyramidal algorithm.

B. Implementation of a Multiresolution Transform

In practice, a physical measuring device can only measure a signal at a finite resolution. For normalization purposes, we suppose that this resolution is equal to 1. Let $A_1^d f$ be the discrete approximation at the resolution 1 that is measured. The causality principle says that from $A_1^d f$ we can compute all the discrete approximations $A_{2^j}^d f$ for $j < 0$. In this section, we describe a simple iterative algorithm for calculating these discrete approximations.

Let $(V_{2^j})_{j \in Z}$ be a multiresolution approximation and $\phi(x)$ be the corresponding scaling function. The family of functions $(\sqrt{2^{-j-1}} \ \phi_{2^{j+1}}(x - 2^{-j-1}k))_{k \in Z}$ is an orthonormal basis of $V_{2^{j+1}}$. We know that for any $n \in Z$, the function $\phi_{2^j}(x - 2^{-j}n)$ is a member of V_{2^j} which is included in $V_{2^{j+1}}$. It can thus be expanded in this orthonormal basis of $V_{2^{j+1}}$:

$$\phi_{2^j}(x - 2^{-j}n) =$$
$$2^{-j-1} \sum_{k=-\infty}^{+\infty} \langle \phi_{2^j}(u - 2^{-j}n), \phi_{2^{j+1}}(u - 2^{-j-1}k) \rangle$$
$$\cdot \phi_{2^{j+1}}(x - 2^{-j-1}k). \quad (13)$$

By changing variables in the inner product integral, one can show that

$$2^{-j-1} \langle \phi_{2^j}(u - 2^{-j}n), \phi_{2^{j+1}}(u - 2^{-j-1}k) \rangle$$
$$= \langle \phi_{2^{-1}}(u), \phi(u - (k - 2n)) \rangle. \quad (14)$$

When computing the inner products of $f(x)$ with both sides of (13) we obtain

$$\langle f(u), \phi_{2^j}(u - 2^{-j}n) \rangle$$
$$= \sum_{k=-\infty}^{+\infty} \langle \phi_{2^{-1}}(u), \phi(u - (k - 2n)) \rangle$$
$$\cdot \langle f(u), \phi_{2^{j+1}}(u - 2^{-j-1}k) \rangle.$$

Let H be the discrete filter whose impulse response is given by

$$\forall n \in Z, \ h(n) = \langle \phi_{2^{-1}}(u), \phi(u - n) \rangle. \quad (15)$$

Let $\tilde{H}$ be the mirror filter with impulse response $\tilde{h}(n) = h(-n)$. By inserting (15) in the previous equation, we

obtain

$$\langle f(u), \phi_{2^j}(u - 2^{-j}n)\rangle$$

$$= \sum_{k=-\infty}^{+\infty} \tilde{h}(2n - k)\,\langle f(u), \phi_{2^{j+1}}(u - 2^{-j-1}k)\rangle.$$

(16)

Equation (16) shows that $A_{2^j}^d f$ can be computed by convolving $A_{2^{j+1}}^d f$ with $\tilde{H}$ and keeping every other sample of the output. All the discrete approximations $A_{2^j}^d f$, for $j < 0$, can thus be computed from $A_1^d f$ by repeating this process. This operation is called a pyramid transform. The algorithm is illustrated by a block diagram in Fig. 5.

In practice, the measuring device gives only a finite number of samples: $A_1^d f = (\alpha_n)_{1 \le n \le N}$. Each discrete signal $A_{2^j}^d f (j < 0)$ has $2^j N$ samples. In order to avoid border problems when computing the discrete approximations $A_{2^j}^d f$, we suppose that the original signal $A_1^d f$ is symmetric with respect to $n = 0$ and $n = N$

$$\alpha_n = \begin{cases} \alpha_{-n} & \text{if } -N < n < 0 \\ \alpha_{2N-n} & \text{if } 0 < n < 0. \end{cases}$$

If the impulse response of the filter $\tilde{H}$ is even ($\tilde{H} = H$), each discrete approximation $A_{2^j}^d f$ will also be symmetric with respect to $n = 0$ and $n = 2^{-j}N$. Fig. 2(a) shows the discrete approximated signal $A_{2^j}^d f$ of a continuous signal $f(x)$ at the resolutions 1, 1/2, 1/4, 1/8, 1/16, and 1/32. These discrete approximated signals have been computed with the algorithm previously described. Appendix A gives the coefficients of the filter H that we used. The continuous approximated signals $A_{2^j}f(x)$ shown in Fig. 2(b) have been calculated by interpolating the discrete approximations with (10). As the resolution decreases, the smaller details of $f(x)$ gradually disappear.

Theorem 1 shows that a multiresolution approximation $(V_{2^j})_{j \in Z}$ is completely characterized by the scaling function $\phi(x)$. A scaling function can be defined as a function $\phi(x) \in L^2(R)$ such that, for all $j \in Z$, $(\sqrt{2^{-j}}\,\phi_{2^j}(x - 2^{-j}n))_{n \in Z}$ is an orthonormal family, and if V_{2^j} is the vector space generated by this family of functions, then $(V_{2^j})_{j \in Z}$ is a multiresolution approximation of $L^2(R)$. We also impose a regularity condition on scaling functions. A scaling function $\phi(x)$ must be continuously differentiable and the asymptotic decay of $\phi(x)$ and $\phi'(x)$ at infinity must satisfy

$$|\phi(x)| = O(x^{-2}) \quad \text{and} \quad |\phi'(x)| = O(x^{-2}).$$

The following theorem gives a practical characterization of the Fourier transform of a scaling function.

Theorem 2: Let $\phi(x)$ be a scaling function, and let H be a discrete filter with impulse response $h(n) = \langle \phi_{2^{-1}}(u), \phi(u - n)\rangle$. Let $H(\omega)$ be the Fourier series defined by

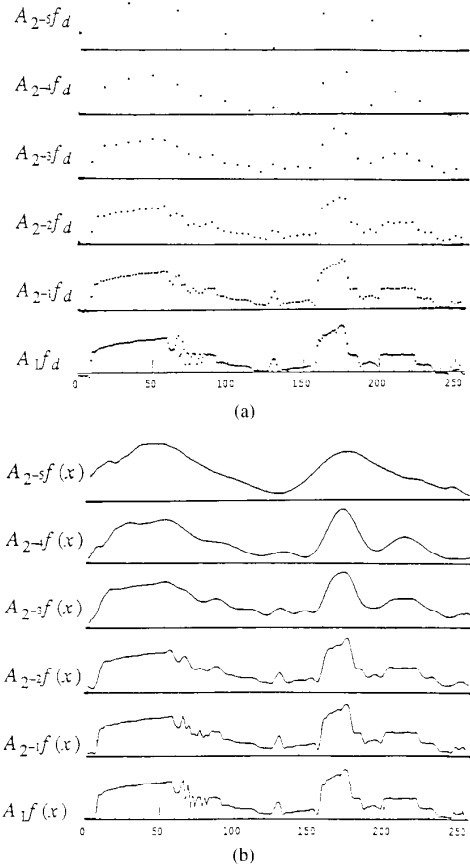$$H(\omega) = \sum_{n=-\infty}^{+\infty} h(n)e^{-in\omega}.$$

(17)

(a)

(b)

Fig. 2. (a) Discrete approximations $A_{2^j}^d f$ at the resolutions 1. 1/2. 1/4. 1/8. 1/16. and 1/32. Each dot gives the amplitude of the inner product $\langle f(u), \phi_{2^j}(u - 2^{-j}n)\rangle$ depending upon $2^{-j}n$. (b) Continuous approximations $A_{2^j}f(x)$ at the resolutions 1. 1/2. 1/4. 1/8. 1/16. and 1/32. These approximations are computed by interpolating the discrete approximations with (10).

$H(\omega)$ satisfies the following two properties:

$$|H(0)| = 1 \quad \text{and} \quad h(n) = O(n^{-2}) \text{ at infinity.} \quad (17a)$$

$$|H(\omega)|^2 + |H(\omega + \pi)|^2 = 1. \quad (17b)$$

Conversely let $H(\omega)$ be a Fourier series satisfying (17a) and (17b) and such that

$$|H(\omega)| \ne 0 \quad \text{for} \quad \omega \in [0, \pi/2]. \quad (17c)$$

The function defined by

$$\hat{\phi}(\omega) = \prod_{p=1}^{+\infty} H(2^{-p}\omega) \quad (18)$$

is the Fourier transform of a scaling function. ∎

Indication for the proof of this theorem are given in Appendix C. The filters that satisfy property (17b) are called *conjugate* filters. One can find extensive descriptions of such filters and numerical methods to synthesize them in the signal processing literature [10], [36], [40]. Given a conjugate filter H which satisfies (17a)–(17c), we can then compute the Fourier transform of the corre-

sponding scaling function with (16). It is possible to choose $H(\omega)$ in order to obtain a scaling function $\phi(x)$ which has good localization properties in both the frequency and spatial domains. The smoothness class of $\phi(x)$ and its asymtotic decay at infinity can be estimated from the properties of $H(\omega)$ [9]. In the multiresolution approximation given in the example of Section II-A, we saw that the scaling function is the indicator function of the interval [0, 1]. One can easily show that the corresponding function $H(\omega)$ satisfies

$$H(\omega) = e^{-i\omega} \cos\left(\frac{\omega}{2}\right).$$

Appendix A describes a class of symmetric scaling functions which decay exponentially and whose Fourier transforms decrease as $1/\omega^n$, for some $n \in N$. Fig. 3 shows the filter H associated with the scaling function given in Fig. 1. This filter is further described in Appendix A.

III. The Wavelet Representation

As explained in the introduction, we wish to build a multiresolution representation based on the differences of information available at two successive resolutions 2^j and 2^{j+1}. This section shows that such a representation can be computed by decomposing the signal using a wavelet orthonormal basis.

A. The Detail Signal

Here, we explain how to extract the difference of information between the approximation of a function $f(x)$ at the resolutions 2^{j+1} and 2^j. This difference of information is called the *detail signal* at the resolution 2^j. The approximation at the resolution 2^{j+1} and 2^j of a signal are respectively equal to its orthogonal projection on $V_{2^{j+1}}$ and V_{2^j}. By applying the projection theorem, we can easily show that the detail signal at the resolution 2^j is given by the orthogonal projection of the original signal on the orthogonal complement of V_{2^j} in $V_{2^{j+1}}$. Let O_{2^j} be this orthogonal complement, i.e.,

$$O_{2^j} \text{ is orthogonal to } V_{2^j},$$

$$O_{2^j} \oplus V_{2^j} = V_{2^{j+1}}.$$

To compute the orthogonal projection of a function $f(x)$ on O_{2^j}, we need to find an orthonormal basis of O_{2^j}. Much like Theorem 1, Theorem 3 shows that such a basis can be built by scaling and translating a function $\psi(x)$.

Theorem 3: Let $(V_{2^j})_{j \in Z}$ be a multiresolution vector space sequence, $\phi(x)$ the scaling function, and H the corresponding conjugate filter. Let $\psi(x)$ be a function whose Fourier transform is given by

$$\hat{\psi}(\omega) = G\left(\frac{\omega}{2}\right) \hat{\phi}\left(\frac{\omega}{2}\right)$$

$$\text{with } G(\omega) = e^{-i\omega} \overline{H(\omega + \pi)}. \quad (19)$$
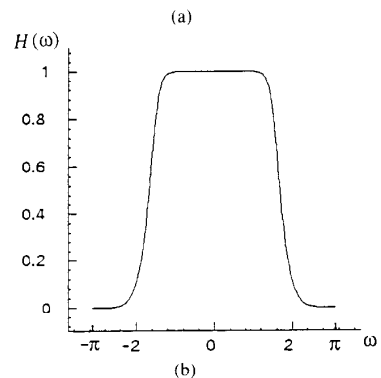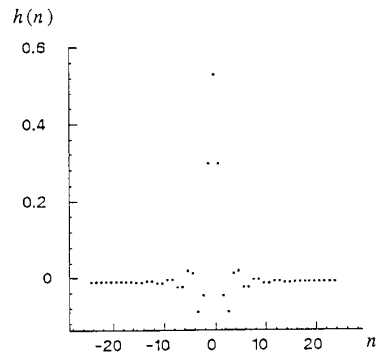

Fig. 3. (a) Impulse response of the filter H associated to the scaling function shown in Fig. 1. The coefficients of this filter are given in Appendix A. (b) Transfer function $H(\omega)$ of the filter H.

Let $\psi_{2^j}(x) = 2^j \psi(2^j x)$ denote the dilation of $\psi(x)$ by 2^j. Then

$$\left(\sqrt{2^{-j}} \, \psi_{2^j}(x - 2^{-j}n)\right)_{n \in Z} \text{ is an orthonormal basis of } O_{2^j}$$

and

$$\left(\sqrt{2^{-j}} \, \psi_{2^j}(x - 2^{-j}n)\right)_{(n,j) \in Z^2}$$

is an orthonormal basis of $L^2(R)$.

$\psi(x)$ is called an *orthogonal wavelet*. ∎

Indications for the proof of this theorem can be found in Appendix D. An orthonormal basis of O_{2^j} can thus be computed by scaling the wavelet $\psi(x)$ with a coefficient 2^j and translating it on a grid whose interval is proportional to 2^{-j}. The wavelet function corresponding to the example of multiresolution given in Section II-A is the Haar wavelet

$$\psi(x) = \begin{cases} 1 & \text{if } 0 \le x < \frac{1}{2} \\ -1 & \text{if } \frac{1}{2} \le x < 1 \\ 0 & \text{otherwise} \end{cases}.$$

This wavelet is not even continuous. In many applications, we want to use a smooth wavelet. For computing a wavelet, we can define a function $H(\omega)$ which satisfies the conditions (17a)–(17c) of Theorem 2, compute the corresponding scaling function $\phi(x)$ with equation (18)

and the wavelet $\psi(x)$ with (19). Depending upon choice of $H(\omega)$, the scaling function $\phi(x)$ and the wavelet $\psi(x)$ can have good localization both in the spatial and Fourier domains. Daubechies [9] studied the properties of $\phi(x)$ and $\psi(x)$ depending upon $H(\omega)$. The first wavelets found by Meyer [35] are both C^∞ and have an asymptotic decay which falls faster than the multiplicative inverse of any polynomial. Daubechies shows that for any $n > 0$, we can find a function $H(\omega)$ such that the corresponding wavelet $\psi(x)$ has a compact support and is n times continuously differentiable [9]. The wavelets described in Appendix A are exponentially decreasing and are in C^n for different values of n. These particular wavelets have been studied by Lemarie [24] and Battle [3].

The decomposition of a signal in an orthonormal wavelet basis gives an intermediate representation between Fourier and spatial representations. The properties of the wavelet orthonormal bases are discussed by Meyer in an advanced functional analysis book [34]. Due to this double localization in the Fourier and the spatial domains, it is possible to characterize the local regularity of a function $f(x)$ based on the coefficients in a wavelet orthonormal basis expansion [25]. For example, from the asymptotic rate of decrease of the wavelet coefficients, we can determine whether a function $f(x)$ is n times differentiable at a point x_0. Fig. 4 shows the wavelet associated with the scaling function of Fig. 1. This wavelet is symmetric with respect to the point $x = 1/2$. The energy of a wavelet in the Fourier domain is essentially concentrated in the intervals $[-2\pi, -\pi] \cup [\pi, 2\pi]$.

Let $P_{O_{2^j}}$ be the orthogonal projection on the vector space O_{2^j}. As a consequence of Theorem 3, this operator can now be written

$$P_{O_2} f(x) = 2^{-j} \sum_{n=-\infty}^{+\infty} \langle f(u), \psi_{2^j}(u - 2^{-j}n) \rangle$$
$$\cdot \psi_{2^j}(x - 2^{-j}n). \tag{20}$$

$P_{O_2} f(x)$ yields to the detail signal of $f(x)$ at the resolution 2^j. It is characterized by the set of inner products

$$D_{2^j}f = \left(\langle f(u), \psi_{2^j}(u - 2^{-j}n) \rangle \right)_{n \in Z}. \tag{21}$$

$D_{2^j}f$ is called the *discrete detail signal* at the resolution 2^j. It contains the difference of information between $A^d_{2^{j-1}}f$ and $A^d_{2^j}f$. As we did in (12), we can prove that each of these inner products is equal to the convolution of $f(x)$ with $\psi_{2^j}(-x)$ evaluated at $2^{-j}n$

$$\langle f(u), \psi_{2^j}(u - 2^{-j}n) \rangle = (f(u) * \psi_{2^j}(-u))(2^{-j}n). \tag{22}$$

Equations (21) and (22) show that the discrete detail signal at the resolution 2^j is equal to a uniform sampling of $(f(u) * \psi_{2^j}(-u))(x)$ at the rate 2^j

$$D_{2^j}f = \left((f(u) * \psi_{2^j}(-u))(2^{-j}n) \right)_{n \in Z}.$$

The wavelet $\psi(x)$ can be viewed as a bandpass filter whose frequency bands are approximatively equal to

(a)

(b)

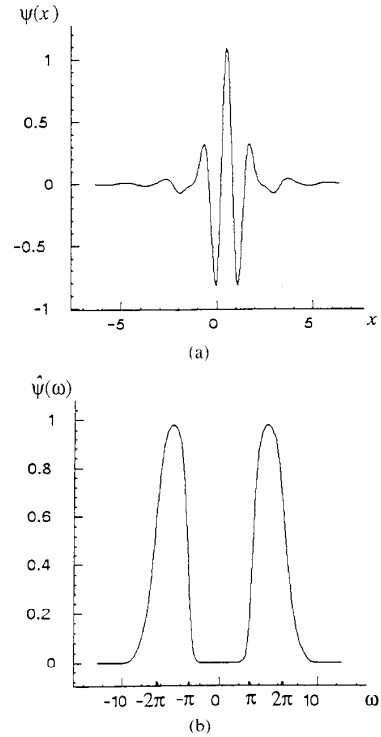Fig. 4. (a) Wavelet $\psi(x)$ associated to the scaling function of Fig. 1. (b) Modulus of the Fourier transform of $\psi(x)$. A wavelet is a band-pass filter.

$[-2\pi, -\pi] \cup [\pi, 2\pi]$. Hence, the detail signal $D_{2^j}f$ describes $f(x)$ in the frequency bands $[-2^{-j+1}\pi, -2^{-j}\pi] \cup [2^{-j}\pi, 2^{-j+1}\pi]$.

We can prove by induction that for any $J > 0$, the original discrete signal $A^d_1 f$ measured at the resolution 1 is represented by

$$\left(A^d_{2^{-J}}f, (D_{2^j}f)_{-J \le j \le -1} \right). \tag{23}$$

This set of discrete signals is called an *orthogonal wavelet representation*, and consists of the reference signal at a coarse resolution $A^d_{2^{-J}}f$ and the detail signals at the resolutions 2^j for $-J \le j \le -1$. It can be interpreted as a decomposition of the original signal in an orthonormal wavelet basis or as a decomposition of the signal in a set of *independent* frequency channels as in Marr's human vision model [30]. The independence is due to the orthogonality of the wavelet functions.

It is difficult to give a precise interpretation of the model in terms of a frequency decomposition because the overlap of the frequency channels. However, we can control this overlap thanks to the orthogonality of our decomposition functions. That is why the tools of functional analysis give a better understanding of this decomposition. If we ignore the overlapping spectral supports, the interpretation in the frequency domain provides an intuitive approach to the model. In analogy with the Laplacian pyramid data structure, $A^d_{2^{-J}}f$ provides the top-level Gaussian pyramid data, and the $D_{2^j}f$ data provide the successive

Laplacian pyramid levels. Unlike the Laplacian pyramid, however, there is no oversampling, and the individual coefficients in the set of data are independent.

B. Implementation of an Orthogonal Wavelet Representation

In this section, we describe a pyramidal algorithm to compute the wavelet representation. With the same derivation steps as in Section II-B, we show that $D_{2^j}f$ can be calculated by convolving $A^d_{2^{j+1}}f$ with a discrete filter G whose form we will characterize.

For any $n \in Z$, the function $\psi_{2^j}(x - 2^{-j}n)$ is a member of $O_{2^j} \subset V_{2^{j+1}}$. In the same manner as (13), this function can be expanded in an orthonormal basis of $V_{2^{j+1}}$

$$\psi_{2^j}(x - 2^{-j}n) =$$

$$2^{-j-1} \sum_{k=-\infty}^{+\infty} \left\langle \psi_{2^j}(u - 2^{-j}n), \phi_{2^{j+1}}(u - 2^{-j-1}k) \right\rangle$$

$$\cdot \phi_{2^{j+1}}(x - 2^{-j-1}k). \tag{24}$$

As we did in (14), by changing variables in the inner product integral we can prove that

$$2^{-j-1} \left\langle \psi_{2^j}(u - 2^{-j}n), \phi_{2^{j+1}}(u - 2^{-j-1}k) \right\rangle$$

$$= \left\langle \psi_{2^{-1}}(u), \phi(u - (k - 2n)) \right\rangle. \tag{25}$$

Hence, by computing the inner product of $f(x)$ with the functions of both sides of (24), we obtain

$$\left\langle f(u), \psi_{2^j}(u - 2^{-j}n) \right\rangle$$

$$= \sum_{k=-\infty}^{+\infty} \left\langle \psi_{2^{-1}}(u), \phi(u - (k - 2n)) \right\rangle$$

$$\cdot \left\langle f(u), \phi_{2^{j+1}}(u - 2^{-j-1}k) \right\rangle. \tag{26}$$

Let G be the discrete filter with impulse response

$$g(n) = \left\langle \psi_{2^{-1}}(u), \phi(u - n) \right\rangle, \tag{27}$$

and $\tilde{G}$ be the symmetric filter with impulse response $\tilde{g}(n) = g(-n)$. We show in Appendix D that the transfer function of this filter is the function $G(\omega)$ defined in Theorem 3, equation (19). Inserting (27) to (26) yields

$$\left\langle f(u), \psi_{2^j}(u - 2^{-j}n) \right\rangle$$

$$= \sum_{k=-\infty}^{+\infty} \tilde{g}(2n - k) \left\langle f(u), \phi_{2^{j+1}}(u - 2^{-j-1}k) \right\rangle. \tag{28}$$

Equation (28) shows that we can compute the detail signal $D_{2^j}f$ by convolving $A^d_{2^{j+1}}f$ with the filter $\tilde{G}$ and retaining every other sample of the output. The orthogonal wavelet representation of a discrete signal $A^d_1 f$ can therefore be computed by successively decomposing $A^d_{2^{j+1}}f$ into $A^d_{2^j}f$ and $D_{2^j}f$ for $-J \le j \le -1$. This algorithm is illustrated by the block diagram shown in Fig. 5.

In practice, the signal $A^d_1 f$ has only a finite number of samples. One method of handling the border problems
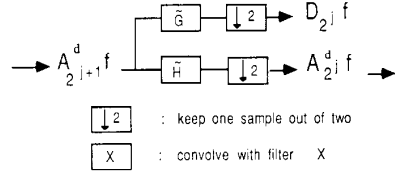

Fig. 5. Decomposition of a discrete approximation $A^d_{2^{j+1}}f$ into an approximation at a coarser resolution $A^d_{2^j}f$ and the signal detail $D_{2^j}f$. By repeating in cascade this algorithm for $-1 \ge j \ge -J$, we compute the wavelet representation of a signal $A^d_1 f$ on J resolution levels.

uses a symmetry with respect to the first and the last sample as in Section II-B.

Equation (19) of Theorem 3 implies that the impulse response of the filter G is related to the impulse response of the filter H by

$$g(n) = (-1)^{1-n} h(1 - n). \tag{29}$$

This equation is provided in Appendix D. G is the *mirror filter* of H, and is a high-pass filter. In signal processing, G and H are called *quadrature mirror* filters [10]. Equation (28) can be interpreted as a high-pass filtering of the discrete signal $A^d_{2^{j+1}}f$.

If the original signal has N samples, then the discrete signals $D_{2^j}f$ and $A^d_{2^j}f$ have $2^j N$ samples each. Thus, the wavelet representation

$$\left(A^d_{2^{-J}}f, (D_{2^j}f)_{-J \le j \le -1} \right)$$

has the same total number of samples as the original approximated signal $A^d_1 f$. This occurs because the representation is orthogonal. Fig. 6(b) gives the wavelet representation of the signal $A^d_1 f$ decomposed in Fig. 2. The energy of the samples of $D_{2^j}f$ gives a measure of the irregularity of the signal at the resolution 2^{j+1}. Whenever $A_{2^j}f(x)$ and $A_{2^{j+1}}f(x)$ are significantly different, the signal detail has a high amplitude. In Fig. 6, this behavior is observed in the textured area between the abscissa coordinates of 60 and 80.

C. Signal Reconstruction from an Orthogonal Wavelet Representation

We have seen that the wavelet representation is complete. We now show that the original discrete signal can also be reconstructed with a pyramid transform. Since O_{2^j} is the orthogonal complement of V_{2^j} in $V_{2^{j+1}}$, $(\sqrt{2^{-j}}$ $\phi_{2^j}(x - 2^{-j}n), \sqrt{2^{-j}} \psi_{2^j}(x - 2^{-j}n))_{n \in Z}$ is an orthonormal basis of $V_{2^{j+1}}$. For any $n > 0$, the function $\phi_{2^{j+1}}(x - 2^{-j-1}n)$ can thus be decomposed in this basis

$$\phi_{2^{j+1}}(x - 2^{-j-1}n)$$

$$= 2^{-j} \sum_{k=-\infty}^{+\infty} \left\langle \phi_{2^j}(u - 2^{-j}k), \phi_{2^{j+1}}(u - 2^{-j-1}n) \right\rangle$$

$$\cdot \phi_{2^j}(x - 2^{-j}k)$$

$$+ 2^{-j} \sum_{k=-\infty}^{+\infty} \left\langle \psi_{2^j}(u - 2^{-j}k), \phi_{2^{j+1}}(u - 2^{-j-1}n) \right\rangle$$
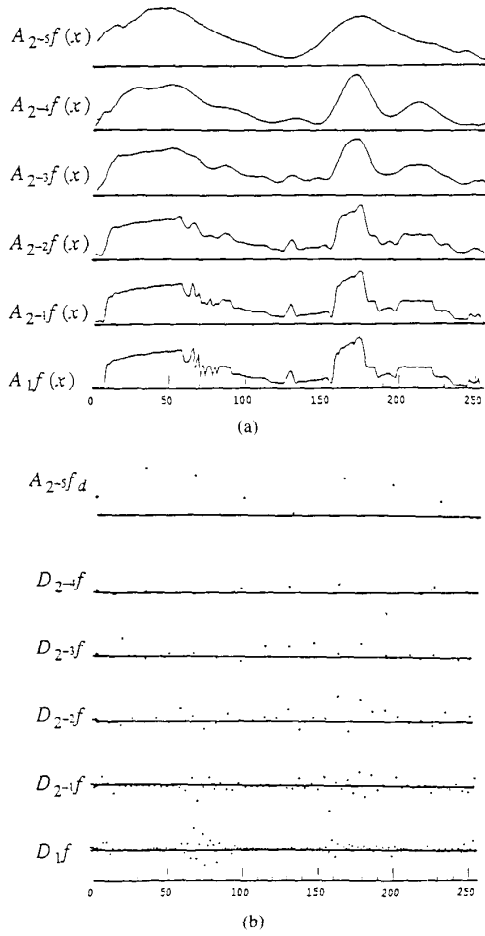
$$\cdot \psi_{2^j}(x - 2^{-j}k). \tag{30}$$

(a)

(b)

Fig. 6. (a) Multiresolution continuous approximations $A_{2^j}f(x)$. (b) Wavelet representation of the signal $A_1 f(x)$. The dots give the amplitude of the inner products $\langle f(u), \psi_{2^j}(u - 2^{-j}n) \rangle$ of each detail signal $D_{2^j}f$ depending upon $2^{-j}n$. The detail signals samples have a high amplitude when the approximations $A_{2^j}f(x)$ and $A_{2^{j+1}}f(x)$ shown in (a) are locally different. The top graph gives the inner products $\langle f(u), \phi_{2^{-j}}(u - 2^j n) \rangle$ of the coarse discrete approximation $A_{2^{-J}}^d f$.

By computing the inner product of each side of equation (30) with the function $f(x)$, we have

$$\langle f(u), \phi_{2^{j+1}}(u - 2^{-j-1}n) \rangle$$

$$= 2^{-j} \sum_{k=-\infty}^{+\infty} \langle \phi_{2^j}(u - 2^{-j}k), \phi_{2^{j+1}}(u - 2^{-j-1}n) \rangle$$

$$\cdot \langle f(u), \phi_{2^j}(u - 2^{-j}k) \rangle$$

$$+ 2^{-j} \sum_{k=-\infty}^{+\infty} \langle \psi_{2^j}(u - 2^{-j}k), \phi_{2^{j+1}}(u - 2^{-j-1}n) \rangle$$

$$\cdot \langle f(u), \psi_{2^j}(u - 2^{-j}k) \rangle. \quad (31)$$

Inserting (14) and (25) in this expression and using the filters H and G, respectively, defined by (15) and (27)
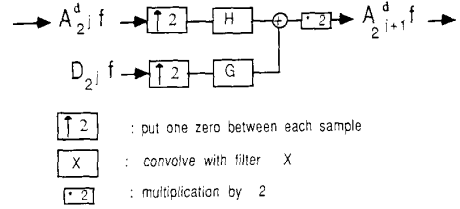

Fig. 7. Reconstruction of a discrete approximation $A_{2^{j+1}}^d f$ from an approximation at a coarser resolution $A_{2^j}^d f$ and the signal detail $D_{2^j}f$. By repeating in cascade this algorithm for $-J \leq j \leq -1$, we reconstruct $A_1^d f$ from its wavelet representation.

yields

$$\langle f(u), \phi_{2^{j+1}}(u - 2^{-j-1}n) \rangle$$

$$= 2 \sum_{k=-\infty}^{+\infty} h(n - 2k) \langle f(u), \phi_{2^j}(u - 2^{-j}k) \rangle$$

$$+ 2 \sum_{k=-\infty}^{+\infty} g(n - 2k) \langle f(u), \psi_{2^j}(u - 2^{-j}k) \rangle. \quad (32)$$

This equation shows that $A_{2^{j+1}}^d f$ can be reconstructed by putting zeros between each sample of $A_{2^j}^d f$ and $D_{2^j}f$ and convolving the resulting signals with the filters H and G, respectively. A quite similar process can be found in the reconstruction algorithm of Burt and Adelson from their Laplacian pyramid [5].

The block diagram shown in Fig. 7 illustrates this algorithm. The original discrete signal $A_1^d f$ at the resolution 1 is reconstructed by repeating this procedure for $-J \leq j < 0$. From the discrete approximation $A_1^d f$, we can recover the continuous approximation $A_1 f(x)$ with equation (10). Fig. 8(a) is a reconstruction of the signal $A_1 f(x)$ from the wavelet representation given in Fig. 6(b). By comparing this reconstruction with the original signal shown in Fig. 8(b), we can appreciate the quality of the reconstruction. The low and high frequencies of the signal are reconstructed well, illustrating the numerical stability of the decomposition and reconstruction processes.

IV. EXTENSION OF THE ORTHOGONAL WAVELET REPRESENTATION TO IMAGES

The wavelet model can be easily generalized to any dimension $n > 0$ [33]. In this section, we study the two-dimensional case for image processing applications. The signal is now a finite energy function $f(x, y) \in L^2(R^2)$. A multiresolution approximation of $L^2(R^2)$ is a sequence of subspaces of $L^2(R^2)$ which satisfies a straightforward two-dimensional extension of the properties (2) to (8). Let $(V_{2^j})_{j \in Z}$ be such a multiresolution approximation of $L^2(R^2)$. The approximation of a signal $f(x, y)$ at a resolution 2^j is equal to its orthogonal projection on the vector space V_{2^j}. Theorem 1 is still valid in two dimensions, and one can show that there exists a unique scaling function $\Phi(x, y)$ whose dilation and translation given an or-
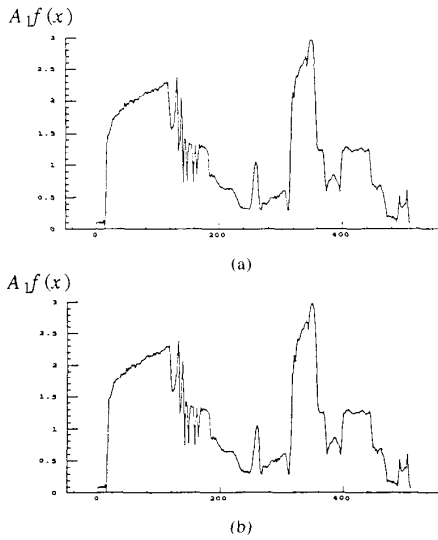
$A_1 f(x)$

(a)

$A_1 f(x)$

(b)

Fig. 8. (a) Original signal $A_1 f(x)$ approximated at the resolution 1. (b) Reconstruction of $A_1 f(x)$ from the wavelet representation shown in Fig. 6(b). By comparing both figures, we can appreciate the quality of the reconstruction.

thonormal basis of each space V_{2^j}. Let $\Phi_{2^j}(x, y) = 2^{2j}$ $\Phi(2^j x, 2^j y)$. The family of functions

$$\left(2^{-j}\Phi_{2^j}(x - 2^{-j}n, y - 2^{-j}m)\right)_{(n,m)\in Z^2}$$

forms an orthonormal basis of V_{2^j}. The factor 2^{-j} normalizes each function in the $L^2(R^2)$ norm. The function $\Phi(x, y)$ is unique with respect to a particular multiresolution approximation of $L^2(R^2)$.

We next describe the particular case of separable multiresolution approximations of $L^2(R^2)$ studied by Meyer [35]. For such multiresolution approximations, each vector space V_{2^j} can be decomposed as a tensor product of two identical subspaces of $L^2(R)$

$$V_{2^j} = V_{2^j}^1 \otimes V_{2^j}^1.$$

The sequence of vector spaces $(V_{2^j})_{j\in Z}$ forms a multiresolution approximation of $L^2(R^2)$ if and only if $(V_{2^j}^1)_{j\in Z}$ is a multiresolution approximation of $L^2(R)$. One can then easily show that the scaling function $\Phi(x, y)$ can be written as

$$\Phi(x, y) = \phi(x)\phi(y)$$

where $\phi(x)$ is the one-dimensional scaling function of the multiresolution approximation $(V_{2^j}^1)_{j\in Z}$. With a separable multiresolution approximation, extra importance is given to the horizontal and vertical directions in the image. For many types of images, such as those from man-made environments, this emphasis is appropriate. The orthogonal basis of V_{2^j} is then given by

$$\left(2^{-j}\Phi_{2^j}(x - 2^{-j}n, y - 2^{-j}m)\right)_{(n,m)\in Z^2}$$
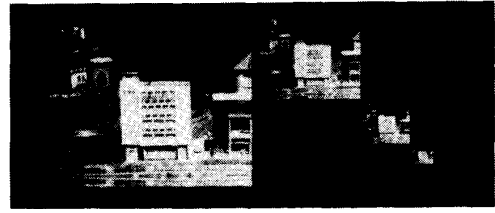$$= \left(2^{-j}\phi_{2^j}(x - 2^{-j}n)\,\phi_{2^j}(y - 2^{-j}m)\right)_{(n,m)\in Z^2}.$$

(33)

Fig. 9. Approximations of an image at the resolutions 1, 1/2, 1/4, and 1/8 ($j = 0, -1, -2, -3$).

The approximation of a signal $f(x, y)$ at a resolution 2^j is therefore characterized by the set of inner products

$$A_{2^j}^d f =$$
$$\left(\langle f(x, y), \phi_{2^j}(x - 2^{-j}n)\,\phi_{2^j}(y - 2^{-j}m)\rangle\right)_{(n,m)\in Z^2}.$$

Let us suppose that the camera measures an approximation of the irradiance of a scene at the resolution 1. Let $A_1^d f$ be the resulting image and N be the number of pixels. One can easily show that for $j < 0$, a discrete image approximation $A_{2^j}^d f$ has $2^{2j}N$ pixels. Border problems are handled by supposing that the original image is symmetric with respect to the horizontal and vertical borders. Fig. 9 gives the discrete approximations of an image at the resolutions 1, 1/2, 1/4, and 1/8.

As in the one-dimensional case, the detail signal at the resolution 2^j is equal to the orthogonal projection of the signal on the orthogonal complement of V_{2^j} in $V_{2^{j+1}}$. Let O_{2^j} be this orthogonal complement. The following theorem gives a simple extension of Theorem 3, and states that we can build an orthonormal basis of O_{2^j} by scaling and translating three wavelets functions, $\Psi^1(x, y)$, $\Psi^2(x, y)$, and $\Psi^3(x, y)$.

Theorem 4: Let $(V_{2^j})_{j\in Z}$ be a separable multiresolution approximation of $L^2(R^2)$. Let $\Phi(x, y) = \phi(x)\phi(y)$ be the associated two-dimensional scaling function. Let $\Psi(x)$ be the one-dimensional wavelet associated with the scaling function $\phi(x)$. Then, the three "wavelets"

$$\Psi^1(x, y) = \phi(x)\psi(y), \quad \Psi^2(x, y) = \psi(x)\phi(y),$$
$$\Psi^3(x, y) = \psi(x)\psi(y)$$

are such that

$$\left(2^{-j}\Psi_{2^j}^1(x - 2^{-j}n, y - 2^{-j}m),\right.$$
$$2^{-j}\Psi_{2^j}^2(x - 2^{-j}n, y - 2^{-j}m),$$
$$\left.2^{-j}\Psi_{2^j}^3(x - 2^{-j}n, y - 2^{-j}m)\right)_{(n,m)\in Z^2} \quad (34)$$

is an orthonormal basis of O_{2^j} and

$$\left(2^{-j}\Psi_{2^j}^1(x - 2^{-j}n, y - 2^{-j}m),\right.$$
$$2^{-j}\Psi_{2^j}^2(x - 2^{-j}n, y - 2^{-j}m),$$
$$\left.2^{-j}\Psi_{2^j}^3(x - 2^{-j}n, y - 2^{-j}m)\right)_{(n,m)\in Z^3} \quad (35)$$

is an orthonormal basis of $L^2(R^2)$.

Appendix E gives a proof of this theorem. The difference of information between $A_{2^{j+1}}^d f$ and $A_{2^j}^d f$ is equal to the orthonormal projection of $f(x)$ on O_{2^j}, and is characterized by the inner products of $f(x)$ with each vector of an orthonormal basis of O_{2^j}. Theorem 4 says that this difference of information is given by the three detail images

$$D_{2^j}^1 f = \left(\langle f(x, y), \Psi_{2^j}^1(x - 2^{-j}n, y - 2^{-j}m) \rangle \right)_{(n,m) \in Z^2},$$
(36)

$$D_{2^j}^2 f = \left(\langle f(x, y), \Psi_{2^j}^2(x - 2^{-j}n, y - 2^{-j}m) \rangle \right)_{(n,m) \in Z^2},$$
(37)

$$D_{2^j}^3 f = \left(\langle f(x, y), \Psi_{2^j}^3(x - 2^{-j}n, y - 2^{-j}m) \rangle \right)_{(n,m) \in Z^2}.$$
(38)

Just as for one-dimensional signals, one can show that in two dimensions the inner products which define $A_{2^j}^d f$, $D_{2^j}^1 f$, $D_{2^j}^2 f$, and $D_{2^j}^3 f$ are equal to a uniform sampling of two-dimensional convolution products. Since the three wavelets $\Psi_1(x, y)$, $\Psi_2(x, y)$, and $\Psi_3(x, y)$ are given by separable products of the functions ϕ and ψ, these convolutions can be written

$$A_{2^j}^d f =$$
$$\left(\left(f(x, y) * \phi_{2^j}(-x) \phi_{2^j}(-y) \right) (2^{-j}n, 2^{-j}m) \right)_{(n,m) \in Z^2}$$
(39)

$$D_{2^j}^1 f =$$
$$\left(\left(f(x, y) * \phi^j(-x) \psi^j(-y) \right) (2^{-j}n, 2^{-j}m) \right)_{(n,m) \in Z^2}$$
(40)

$$D_{2^j}^2 f =$$
$$\left(\left(f(x, y) * \psi_{2^j}(-x) \phi_{2^j}(-y) \right) (2^{-j}n, 2^{-j}m) \right)_{(n,m) \in Z^2}$$
(41)

$$D_{2^j}^3 f =$$
$$\left(\left(f(x, y) * \psi_{2^j}(-x) \psi_{2^j}(-y) \right) (2^{-j}n, 2^{-j}m) \right)_{(n,m) \in Z^2}.$$
(42)

The expressions (39) through (42) show that in two dimensions, $A_{2^j}^d f$ and the $D_{2^j}^k f$ are computed with separable filtering of the signal along the abscissa and ordinate.

The wavelet decomposition can thus be interpreted as a signal decomposition in a set of independent, *spatially oriented* frequency channels. Let us suppose that $\phi(x)$ and $\psi(x)$ are, respectively, a perfect low-pass and a perfect bandpass filter. Fig. 10(a) shows in the frequency domain how the image $A_{2^{j+1}}^d f$ is decomposed into $A_{2^j}^d f$, $D_{2^j}^1 f$, $D_{2^j}^2 f$, and $D_{2^j}^3 f$. The image $A_{2^j}^d f$ corresponds to the lowest frequencies, $D_{2^j}^1 f$ gives the vertical high frequencies (horizontal edges), $D_{2^j}^2 f$ the horizontal high frequencies (vertical edges) and $D_{2^j}^3 f$ the high frequencies in both directions (the corners). This is illustrated by the decomposition of a white square on a black background explained in Fig. 11(b). The arrangement of the $D_{2^j}^k f$ im-
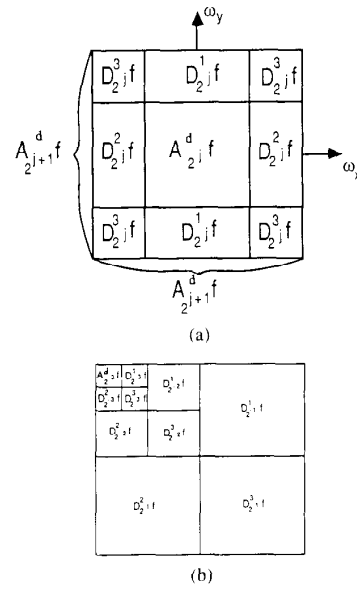

(a)

(b)

Fig. 10. (a) Decomposition of the frequency support of the image $A_{2^{j+1}}^d f$ into $A_{2^j}^d f$ and the detail images $D_{2^j}^k f$. The image $A_{2^j}^d f$ corresponds to the lower horizontal and vertical frequencies of $A_{2^{j+1}}^d f$. $D_{2^j}^1 f$ gives the vertical high frequencies and horizontal low frequencies, $D_{2^j}^2 f$ the horizontal high frequencies and vertical low frequencies, and $D_{2^j}^3 f$ the high frequencies in both horizontal and vertical directions. (b) Disposition of the $D_{2^j}^k f$ and $A_{2^j}^d f$ images of the image wavelet representations shown in this article.

(a)

(b)

(c)
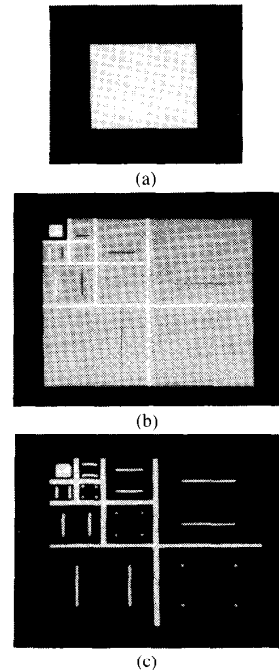
Fig. 11. (a) Original image. (b) Wavelet representation on three resolution levels. The black, grey, and white pixels correspond respectively to negative, zero, and positive wavelet coefficients. The disposition of the detail images is explained in Fig. 10(b). (c) These images show the absolute value of the wavelet coefficients for each detail images $D_{2^j}^k f$ shown in (b). Black and white pixels correspond respectively to zero and high amplitude coefficients. The amplitude is high along the edges of the square for each orientation.

ages is shown in Fig. 10(b). The black, grey, and white pixels respectively correspond to negative, zero, and positive coefficients. Fig. 11(c) shows the absolute value of the detail signal samples. The black pixels correspond to zero whereas the white ones have a high positive value. As expected, the detail signal samples have a high amplitude on the horizontal edges, the vertical edges and the corners of the square.

For any $J > 0$, an image $A_1^d f$ is completely represented by the $3J + 1$ discrete images

$$\left(A_{2^{-J}}^d f, \left(D_{2^j}^1 f\right)_{-J \leq j \leq -1}, \left(D_{2^j}^2 f\right)_{-J \leq j \leq -1},\right.$$

$$\left.\left(D_{2^j}^3 f\right)_{-J \leq j \leq -1}\right).$$

This set of images is called an *orthogonal wavelet representation* in two dimensions. The image $A_{2^{-J}}^d f$ is the coarse approximation at the resolution 2^{-J} and the $D_{2^j}^k f$ images give the detail signals for different orientations and resolutions. If the original image has N pixels, each image $A_{2^j}^d f$, $D_{2^j}^1 f$, $D_{2^j}^2 f$, $D_{2^j}^3 f$ has $2^j N$ pixels ($j < 0$). The total number of pixels in this new representation is equal to the number of pixels of the original image, so we do not increase the volume of data. Once again, this occurs due to the orthogonality of the representation. In a correlated multiresolution representation such as the Laplacian pyramid, the total number of pixels representing the signal is increased by a factor of 2 in one dimension and of 4/3 in two dimensions.

A. Decomposition and Reconstruction Algorithms in Two Dimensions

In two dimensions, the wavelet representation can be computed with a pyramidal algorithm similar to the one-dimensional algorithm described in Section III-B. The two-dimensional wavelet transform that we describe can be seen as a one-dimensional wavelet transform along the x and y axes. By repeating the analysis described in Section III-B, we can show that a two-dimensional wavelet transform can be computed with a separable extension of the one-dimensional decomposition algorithm. At each step we decompose $A_{2^{j+1}}^d f$ into $A_{2^j}^d f$, $D_{2^j}^1 f$, $D_{2^j}^2 f$, and $D_{2^j}^3 f$. This algorithm is illustrated by a block diagram in Fig. 12. We first convolve the rows of $A_{2^{j+1}}^d f$ with a one-dimensional filter, retain every other row, convolve the columns of the resulting signals with another one-dimensional filter and retain every other column. The filters used in this decomposition are the quadrature mirror filters $\tilde{H}$ and $\tilde{G}$ described in Sections II-B and III-B.

The structure of application of the filters for computing $A_{2^j}^d$, $D_{2^j}^1$, $D_{2^j}^2$, and $D_{2^j}^3$ is given in Fig. 12. We compute the wavelet transform of an image $A_1^d f$ by repeating this process for $-1 \geq j \geq -J$. This corresponds to a separable conjugate mirror filter decomposition [44].

Fig. 14(b) shows the wavelet representation of a natural scene image decomposed on 3 resolution levels. The pattern of arrangement of the detail images is as explained in Fig. 10(b). Fig. 14(c) gives the absolute value of the wavelet coefficients of each detail image. The wavelet
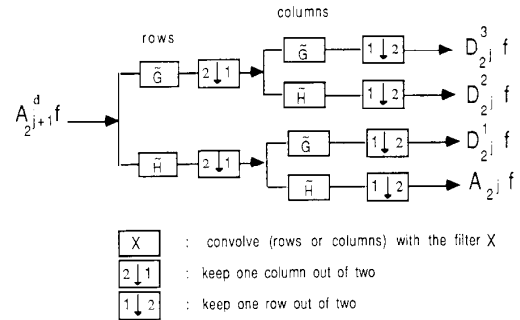
Fig. 12. Decomposition of an image $A_{2^{j+1}}^d f$ into $A_{2^j}^d f$, $D_{2^j}^1 f$, $D_{2^j}^2 f$, and $D_{2^j}^3 f$. This algorithm is based on one-dimensional convolutions of the rows and columns of $A_{2^{j+1}}^d f$ with the one dimensional quadrature mirror filters $\tilde{H}$ and $\tilde{G}$.

coefficients have a high amplitude around the images edges and in the textured areas within a given spatial orientation.

The one-dimensional reconstruction algorithm described in Section III-C can also be extended to two dimensions. At each step, the image $A_{2^{j+1}}^d f$ is reconstructed from $A_{2^j}^d f$, $D_{2^j}^1 f$, $D_{2^j}^2 f$, and $D_{2^j}^3 f$. This algorithm is illustrated by a block diagram in Fig. 13. Between each column of the images $A_{2^j}^d f$, $D_{2^j}^1 f$, $D_{2^j}^2 f$, and $D_{2^j}^3 f$, we add a column of zeros, convolve the rows with a one dimensional filter, add a row of zeros between each row of the resulting image, and convolve the columns with another one-dimensional filter. The filters used in the reconstruction are the quadrature mirror filters H and G described in Sections II-B and III-B. The image $A_1^d f$ is reconstructed from its wavelet transform by repeating this process for $-J \leq j \leq -1$. Fig. 14(d) shows the reconstruction of the original image from its wavelet representation. If we use floating-point precision for the discrete signals in the wavelet representation, the reconstruction is of excellent quality. Reconstruction errors are more thoroughly discussed in the next section.

V. Applications of the Orthogonal Wavelet Representation

A. Compact Coding of Wavelet Image Representations

To compute an exact reconstruction of the original image, we must store the pixel values of each detail image with infinite precision. However, for practical applications, we can allow errors to occur as long as the relevant information is not destroyed for a human observer. In this section, we show how to use the sensitivity of the human visual system as well as the statistical properties of the image to optimize the coding by the wavelet representation. The conjugate mirror filters which implement the wavelet decomposition have also been studied by Woods [44] and Adelson *et al.* [1] for image coding.

Let $\left(A_{2^{-J}}^d f, \left(D_{2^j}^1 f\right)_{-J \leq j \leq -1}, \left(D_{2^j}^2 f\right)_{-J \leq j \leq -1}, \left(D_{2^j}^3 f\right)_{-J \leq j \leq -1}\right)$ be the wavelet representation of an image $A_1^d f$. Let $\left(\epsilon_{-J}, \left(\epsilon_j^1\right)_{-J \leq j \leq -1}, \left(\epsilon_j^2\right)_{-J \leq j \leq -1}, \left(\epsilon_j^3\right)_{-J \leq j \leq -1}\right)$ be the mean square errors introduced when coding each image component of the wavelet representa-

Fig. 13. Reconstruction of an image $A_{2^{j+1}}^d f$ from $A_{2^j}^d f$, $D_{2^j}^1 f$, $D_{2^j}^2 f$, and $D_{2^j}^3 f$. The row and columns of these images are convolved with the one dimensional quadrature mirror filters H and G.
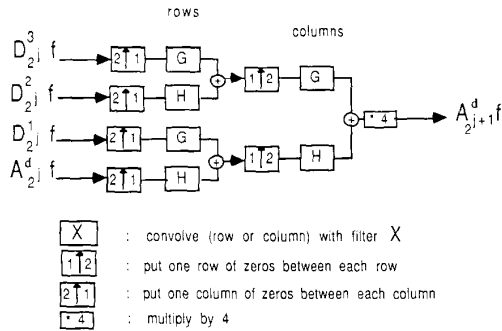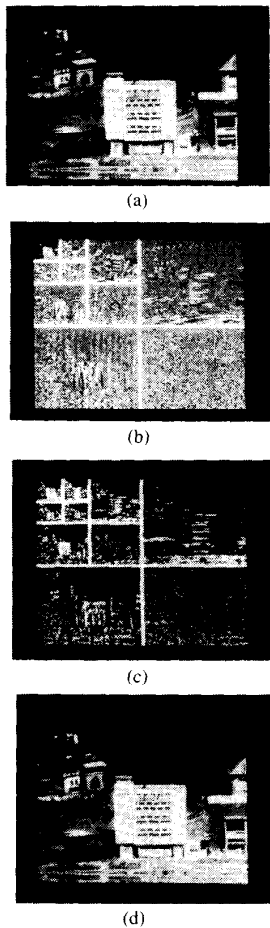

(a)

(b)

(c)

(d)

Fig. 14. (a) Original image. (b) Wavelet representation on three resolution levels. The arrangement of the detail images is explained in Fig. 10(b). (c) These images show the absolute value of the wavelet coefficients for each detail images $D_{2^j}^k$ shown in (b). The amplitude is high along the edges and the textured area for each orientation. (d) Reconstruction of the original image from the wavelet representation given in (b).

tion. Let ϵ_0 be the mean square error of the image reconstructed from the coded wavelet representation. Since the wavelet representation is orthogonal in $L^2(R^2)$, one can

prove that

$$\epsilon_0 = 2^{2J}\epsilon_{-J} + \sum_{k=1}^{3} \sum_{j=-J}^{-1} 2^{-2j}\epsilon_j^k. \tag{43}$$

The factors 2^{-2j} are due to the normalization factor 2^{-j} which appears in (33) and (34). Psychological experiments on human visual sensitivity show that the visible distortion on the reconstructed image will not only depend on the total mean square error ϵ_0, but also on the distribution of this error between the different detail images $D_{2^j}^k f$. The contrast sensitivity function of the visual system [6] shows that the perception of a contrast distortion in the image depends upon the frequency components of the modified contrast. Visual sensitivity also depends upon the orientation of the stimulus. The results of Campbell and Kulikowski [7] show that the human visual system has a maximum sensitivity when the contrast is horizontal or vertical. When the contrast is tilted at $45°$, the sensitivity is minimum. A two-dimensional wavelet representation corresponds to a decomposition of the image into independent frequency bands and three spatial orientations. Each detail image $D_{2^j}^k$ gives the image contrast in a given frequency range and along a particular orientation. It is therefore possible to adapt the coding error of each detail image to the sensitivity of human perception for the corresponding frequency band and spatial orientation selectivity. The more sensitive the human visual system, the less coding error we want to introduce in the detail image $D_{2^j}^k f$. Watson [43] has made a particularly detailed study of subband image coding adapted to human visual perception.

Given an allocation of the coding error between the different resolutions and orientations of the wavelet representation, we must then code each detail image with a minimum number of bytes. In order to optimize the coding, one can use the statistical properties of the wavelet coefficients for each resolution and orientation. Natural images are special kinds of two-dimensional signals. This shows up clearly when one looks at the histogram of the detail images $D_{2^j}^k f$. Since the pixels of these detail images are the decomposition coefficients of the original image in an orthonormal family, they are not correlated. The histogram of the detail images could therefore have any distribution. Yet in practice, for all resolutions and orientations, these histograms are symmetrical peaks centered in zero. Natural images must therefore belong to a particular subset of $L^2(R^2)$. The modeling of this subset is a well known problem in image processing [26]. The wavelet orthonormal bases are potentially helpful for this purpose. Indeed, the statistical properties of an image decomposition in a wavelet orthonormal basis look simpler than the statistical properties of the original image. Moreover, the orthogonality of the wavelet functions can simplify the mathematical analysis of the problem.

We have found experimentally that the detail image histograms can be modeled with the following family of histograms:

$$h(u) = Ke^{-(|u|/\alpha)^\beta}. \tag{44}$$

The parameter β modifies the decreasing rate of the peak and α models the variance. This model was built by studing the histograms of seven different images decomposed on four resolution levels each. Our goal was only to define a qualitative histogram model. The constant K is adjusted in order to have $\int_{-\infty}^{\infty} h(u) \, du = N$ where N is the total number of pixels of the given detail image. By changing variables in the integral, one can derive that

$$K = \frac{N\beta}{2\alpha\Gamma\left(\frac{1}{\beta}\right)}, \quad \text{where} \quad \Gamma(t) = \int_0^{\infty} e^{-u} u^{t-1} \, du. \quad (45)$$

The coefficients α and β of the histogram model can be computed by measuring the first and second moment of the detail image histogram:

$$m_1 = \int_{-\infty}^{\infty} |u| h(u) \, du \quad \text{and} \quad m_2 = \int_{-\infty}^{\infty} u^2 h(u) \, du. \quad (46)$$

By inserting (44) of the histogram model and changing variables in these two integrals, we obtain

$$m_1 = 2K \frac{\alpha^2}{\beta} \Gamma\left(\frac{2}{\beta}\right) \quad \text{and} \quad m_2 = 2K \frac{\alpha^3}{\beta} \Gamma\left(\frac{3}{\beta}\right). \quad (47)$$

Thus,

$$\beta = F^{-1}\left(\frac{m_1^2}{m_2 N}\right) \quad \text{where} \quad F(x) = \frac{\Gamma\left(\frac{2}{x}\right)^2}{\Gamma\left(\frac{3}{x}\right)\Gamma\left(\frac{1}{x}\right)} \quad (48)$$

and

$$\alpha = \frac{m_2\Gamma\left(\frac{1}{\beta}\right)}{N\Gamma\left(\frac{3}{\beta}\right)}. \quad (49)$$

The function $F^{-1}(x)$ is shown in Fig. 15. Fig. 16(a) gives a typical example of a detail image histogram obtained from the wavelet representation of a real image. Fig. 16(b) is the graph of the model derived from (44).

The *a priori* knowledge of the detail signal's statistical distribution given by the histogram model (44) can be used to optimize the coding of these signals. We have developed such a procedure [27] using Max's algorithm [32] to minimize the quantization noise on the wavelet representation. Predictive coding procedures are also effective for this purpose. Results show that one can code an image using such a representation with less than 1.5 bits per pixel with few visible distortions [1], [27], [44].

B. Texture Discrimination and Fractal Analysis

We now describe the application of the wavelet orthogonal representation to texture discrimination and fractal
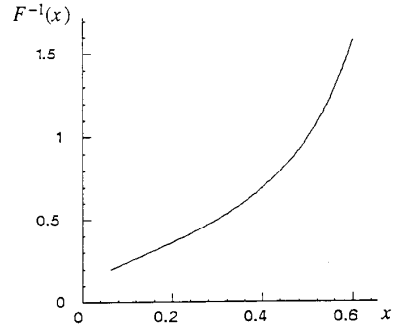

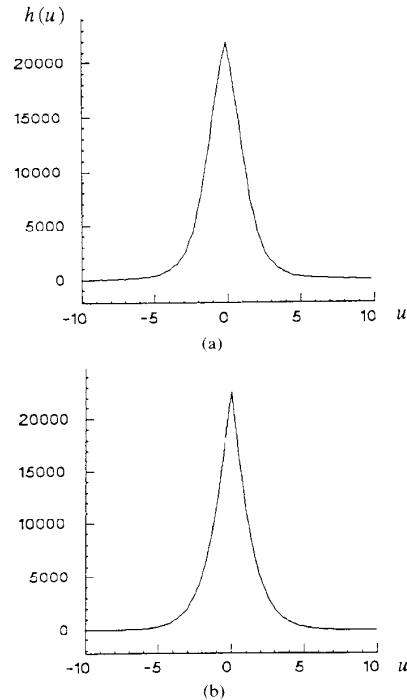Fig. 15. Graph of the function $F^{-1}(x)$ characterized by (49).

Fig. 16. (a) Typical example of a detail image histogram $h(u)$. (b) Modeling of $h(u)$ obtained from equation (44). The parameters α and β have been computed from the first two moments of the original histogram ($\alpha = 1.39$ and $\beta = 1.14$).

analysis. Using psychophysics, Julesz [21] has developed a texture discrimination theory based on the decomposition of textures into basic primitives called *textons*. These textons are spatially local; they have a particular spatial orientation and narrow frequency tuning. The wavelet representation can also be interpreted as a texton decomposition where each texton is equal to a particular function of the wavelet orthonormal basis. Indeed, these functions have all the discriminative abilities required by the Julesz theory. In the decomposition studied in this article, we have used only three orientation tunings. However, one can build a wavelet representation having as many orientation tunings as desired by using non-separable wavelet orthonormal bases [33].

Fig. 17(a) shows three textures synthesized by Beck. Humans cannot preattentively discriminate the middle from the right texture but can separate the left texture from the others. In this example, human discrimination is based mainly on the orientation of these textures as their frequency content is very similar. With a first-order statistical analysis of the wavelet representation shown in Fig. 17(b), we can also discriminate the left texture but not the two others. This example illustrates the ability of our representation to differentiate textures on orientation criteria. This is of course only one aspect of the problem, and a more sophisticated statistical analysis is needed for modeling textures [13]. Although several psychophysical studies have shown the importance of a signal decomposition in several frequency channels [4], [15], there still is no statistical model to combine the information provided by the different channels. From this point of view, the wavelet mathematical model might be helpful to transpose some of the tools currently used in functional analysis to characterize the local regularity of functions [25].

Mandelbrot [29] has shown that certain natural textures can be modeled with Brownian fractal noise. Brownian fractal noise $F(x)$ is a random process whose local differences

$$\frac{\left| F(x) - F(x + \Delta x) \right|}{\left\| \Delta x \right\|^H}$$

has a probability distribution function $g(x)$ which is Gaussian. Such a random process is self-similar, i.e.,

$$\forall r > 0, \ F(x) \ \text{and} \ r^H F(rx) \ \text{are statistically identical.}$$

Hence, a realization of $F(x)$ looks similar at any scale and for any resolution. Fractals do not provide a general model which can be used for the analysis of any kind of texture, but Pentland [39] has shown that for a fractal texture, the psychophysical perception of roughness can be quantified with the fractal dimension.

Fig. 18(a) shows a realization of a fractal noise which looks like a cloud. Its fractal dimension is 2.5. Fig. 18(b) gives the wavelet representation of this fractal. As expected, the detail signals are similar at all resolutions. The image $A_{2^{-3}}^d f$ gives the local dc component of the original fractal image. For a cloud, this would correspond to the local differences of illuminations.

Let us show that the fractal dimension can be computed from the wavelet representation. We give the proof for one-dimensional fractal noise, but the result can be easily extended to two dimensions. The power spectrum of fractal noise is given by [29]

$$P(\omega) = k\omega^{-2H-1}. \tag{50}$$

The fractal dimension is related to the exponent H by

$$D = T + 1 - H \tag{51}$$

where T is the topological dimension of the space in which x varies (for images $T = 2$). Since Brownian fractal noise is not a stationary process, this power spectrum cannot be
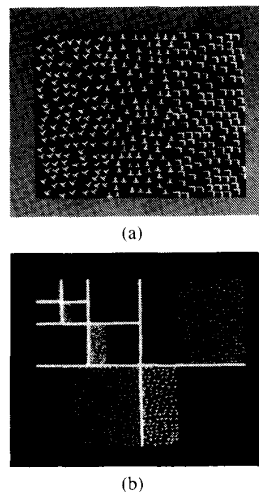

(a)

(b)

Fig. 17. (a) J. Beck textures: only the left texture is preattentively discriminable by a human observer. (b) These images show the absolute value of the wavelet coefficients of image (a). computed on three resolution levels. The left texture can be discriminated with a first-order statistical analysis of the detail signals amplitude. The two other textures can not be discriminated with such a technic.
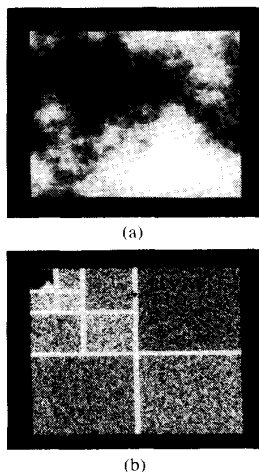

(a)

(b)

Fig. 18. (a) Brownian fractal image. (b) Wavelet representation on three resolution levels of image (a). As expected, the detail signals are similar at all resolutions.

interpreted in the classical sense. Flandrin [12] has shown how to define precisely this power spectrum formula with a time-frequency analysis. We saw in equation (22) that the detail signals $D_{2^j} f$ are obtained by filtering the signal with $\psi_{2^j}(-x)$ and sampling the output. The power spectrum of the fractal filtered by $\psi_{2^j}(-x)$ is given by

$$P_{2^j}(\omega) = P(\omega) \left| \hat{\psi}(2^{-j}\omega) \right|^2. \tag{52}$$

After sampling at a rate 2^j, the power spectrum of the discrete detail signal becomes [37]

$$P_{2^j}^d(\omega) = 2^j \sum_{k=-\infty}^{+\infty} P_{2^j}(\omega + 2^j 2k\pi). \tag{53}$$

Let $\sigma_{2^j}^2$ be the energy of the detail signal $D_{2^j}f$

$$\sigma_{2^j}^2 = \frac{2^{-j}}{2\pi} \int_{-2^j\pi}^{+2^j\pi} P_{2^j}^d(\omega) \, d\omega. \qquad (54)$$

By inserting (52) and (53) into (54) and changing variables in this integral, we obtain that

$$\sigma_{2^j}^2 = 2^{2H}\sigma_{2^{j+1}}^2. \qquad (55)$$

For a fractal, the ratio $\sigma_{2^j}^2/\sigma_{2^{j+1}}^2$ is therefore constant. From the wavelet representation of a Brownian fractal, we compute H from equation (55) and derive the fractal dimension D with (51). This result can easily be extended to two dimensions in order to compute the fractal dimension of fractal images. Analogously, we compute the ratios of the energy of the detail images within each direction, and derive the value of the coefficient H. A similar algorithm has been proposed by Heeger and Pentland for analyzing fractals with Gabor functions [19]. For the fractal shown in Fig. 18(a), we calculated the ratios of the energy of the detail images within each orientation for the resolutions $1/2$, $1/4$, and $1/8$. We recovered the fractal dimension of this image from each of these ratios with a 3 percent maximum error.

Much research work has recently concentrated on the analysis of fractals with the wavelet transform [2]. This topic is promising because multiscale decompositions, such as the wavelet transform, are well adapted to evaluate the self-similarity of a signal and its fractal properties.

VI. Conclusion

This article has described a mathematical model for the computation and interpretation of the concept of a multiresolution representation. We explained how to extract the difference of information between successive resolutions and thus define a new (complete) representation called the wavelet representation. This representation is computed by decomposing the original signal using a wavelet orthonormal basis, and can be interpreted as a decomposition using a set of independent frequency channels having a spatial orientation tuning. A wavelet representation lies between the spatial and Fourier domains. There is no redundant information because the wavelet functions are orthogonal. The computation is efficient due to the existence of a pyramidal algorithm based on convolutions with quadrature mirror filters. The original signal can be reconstructed from the wavelet decomposition with a similar algorithm.

We discussed the application of the wavelet representation to data compression in image coding. We showed that an orthogonal wavelet transform provides interesting insight on the statistical properties of images. The orientation selectivity of this representation is useful for many applications. We reviewed in particular the texture discrimination problem. A wavelet transform is particularly well-suited to analyze the fractal properties of images. Specifically, we showed how to compute the fractal dimension of a Brownian fractal from its wavelet represen-

tation. In this article, we emphasized the computer vision applications, but this representation can also be helpful for pattern recognition in other domains. Grossmann and Kronland-Martinet [23] are currently working on speech recognition applications, and Morlet [14] studies seismic signal analysis. The wavelet orthonormal bases are also studied in both pure and applied mathematics [20], [25], and have found applications in *Quantum Mechanics* with the work of Paul [38] and Federbush [11].

Appendix A
An Example Multiresolution Approximation

In this appendix, we describe a class of multiresolution approximations of $L^2(R)$ studied by Lemarie [24] and Battle [3]. We explain how to compute the corresponding scaling functions $\phi(x)$, wavelets $\psi(x)$, and quadrature filters H. These multiresolution approximations are built from polynomial splines of order $2p + 1$. The vector space V_1 is the vector space of all functions of $L^2(R)$ which are p times continuously differentiable and equal to a polynomial of order $2p + 1$ on each interval $[k, k + 1]$, for any $k \in Z$. The other vector spaces V_{2^j} are derived from V_1 with property (3). Lemarie has shown that the scaling function associated with such a multiresolution approximation can be written

$$\hat{\phi}(\omega) = \frac{1}{\omega^n\sqrt{\Sigma_{2n}(\omega)}} \quad \text{where} \quad n = 2 + 2p, \qquad (56)$$

and where the function $\Sigma_n(\omega)$ is given by

$$\Sigma_n(\omega) = \sum_{k=-\infty}^{+\infty} \frac{1}{(\omega + 2k\pi)^n}. \qquad (57)$$

We can compute a closed form of $\Sigma_n(\omega)$ by calculating the derivative of order $n - 2$ of the equation

$$\Sigma_2(\omega) = \frac{1}{4\sin^2(\omega/2)}.$$

Theorem 2 says that $\hat{\phi}(\omega)$ is related to the transfer function $H(\omega)$ of a quadrature mirror filter by

$$\hat{\phi}(2\omega) = H(\omega)\,\hat{\phi}(\omega).$$

From (56) we obtain

$$H(\omega) = \sqrt{\frac{\Sigma_{2n}(\omega)}{2^{2n}\Sigma_{2n}(2\omega)}}. \qquad (58)$$

The Fourier transform of the corresponding orthonormal wavelet can be derived from the property (19) of Theorem 3

$$\hat{\psi}(\omega) = e^{-i(\omega/2)}\overline{H}\left(\frac{\omega}{2} + \pi\right)\hat{\phi}\left(\frac{\omega}{2}\right)$$

$$= \frac{e^{-i(\omega/2)}}{\omega^n}\frac{\sqrt{\Sigma_{2n}\left(\frac{\omega}{2} + \pi\right)}}{\sqrt{\Sigma_{2n}(\omega)\,\Sigma_{2n}\left(\frac{\omega}{2}\right)}}. \qquad (59)$$

The wavelet $\psi(x)$ defined by (59) decreases exponentially.

The scaling function shown in Fig. 1 was obtained with $p = 1$, and thus $n = 4$. It corresponds to a multiresolution approximation built from cubic splines. Let

$$N_1(\omega) = 5 + 30\left(\cos\frac{\omega}{2}\right)^2 + 30\left(\sin\frac{\omega}{2}\right)^2\left(\cos\frac{\omega}{2}\right)^2$$

and

$$N_2(\omega) = 2\left(\sin\frac{\omega}{2}\right)^4\left(\cos\frac{\omega}{2}\right)^2 + 70\left(\cos\frac{\omega}{2}\right)^4 + \frac{2}{3}\left(\sin\frac{\omega}{2}\right)^6.$$

The function $\Sigma_8(\omega)$ is given by

$$\Sigma_8(\omega) = \frac{N_1(\omega) + N_2(\omega)}{105\left(\sin\frac{\omega}{2}\right)^8}.$$

For this multiresolution approximation based on cubic splines, the functions $\hat{\phi}(\omega)$ and $\hat{\psi}(\omega)$ are computed from (56) and (59) with $n = 4$. The transfer function $H(\omega)$ of the quadrature mirror filter is given by equation (58). Table I gives the first 12 coefficients of the impulse response $(h(n))_{n\in Z}$. This filter is symmetrical. The impulse response of the mirror filter G is obtained with (29).

APPENDIX B
PROOF OF THEOREM 1

This appendix gives the main steps of the proof of Theorem 1. More details can be found in [28]. We prove Theorem 1 for $j = 0$. The result can be extended for any $j \in Z$ using the property (3). From the properties (5) and (6) of the isomorphism I from V_1 onto $I^2(Z)$, one can prove that there exists a function $g(x)$ such that $(g(x - k))_{k\in Z}$ is a basis of V_1. We are looking for a function $\phi(x) \in V_1$ such that $(\phi(x - k))_{k\in Z}$ is an orthonormal basis of V_1. Let $\hat{\phi}(\omega)$ be the Fourier transform of $\phi(x)$. With the Poisson formula, we can show that the family of functions $(\phi(x - k))_{k\in Z}$ is orthonormal if and only if

$$\sum_{k=-\infty}^{+\infty}\left|\hat{\phi}(\omega + 2k\pi)\right|^2 = 1. \tag{60}$$

Since $\phi(x) \in V_1$, it can be decomposed in the basis $(g(x - k))_{k\in Z}$:

$$\exists(\alpha_k)_{k\in Z} \in I^2(Z) \quad \text{such that} \quad \phi(x) = \sum_{-\infty}^{+\infty}\alpha_k g(x - k). \tag{61}$$

The Fourier transform of (61) can be written

$$\hat{\phi}(\omega) = M(\omega)\hat{g}(\omega) \quad \text{with} \quad M(\omega) = \sum_{k=-\infty}^{+\infty}\alpha_k e^{ik\omega}. \tag{62}$$

TABLE I

n	h(n)	n	h(n)
0	0.542	6	0.012
1	0.307	7	-0.013
2	-0.035	8	0.006
3	-0.078	9	0.006
4	0.023	10	-0.003
5	-0.030	11	-0.002

By inserting (62) in (60), we obtain

$$M(\omega) = \left(\sum_{k=-\infty}^{+\infty}\left|\hat{g}(\omega + 2k\pi)\right|^2\right)^{-1/2}. \tag{63}$$

One can show that the continuity of the isomorphism I implies that there exists two constants C_1 and C_2 such that

$$C_1 \leq \left(\sum_{-\infty}^{+\infty}\left|\hat{g}(\omega + 2k\pi)\right|^2\right)^{1/2} \leq C_2.$$

Hence, (63) is defined for any $\omega \in R$. Conversely, it is simple to prove that equations (62) and (63) define the Fourier transform of a function $\phi(x)$ such that $(\phi(x - k))_{k\in Z}$ is an orthonormal family that generates V_1.

APPENDIX C
PROOF OF THEOREM 2

This appendix gives the main steps of the proof of Theorem 2. More details can be found in [28]. Let us first prove property (17a). Since $\phi_{2^{-1}}(x) \in V_{-1} \subset V_1$, it can be decomposed in the orthogonal basis $(\phi(x - k))_{k\in Z}$

$$\phi_{2^{-1}}(x) = \sum_{k=-\infty}^{+\infty}\langle\phi_{2^{-1}}(u), \phi(u - k)\rangle\,\phi(u - k).$$

The Fourier transform of this equation yields

$$\hat{\phi}(2\omega) = H(\omega)\hat{\phi}(\omega) \tag{64}$$

where $H(\omega)$ is the Fourier series defined by (17). One can show that the property (7) of a multiresolution approximation implies that any scaling function satisfies

$$\left|\int_{-\infty}^{+\infty}\phi(x)\,dx\right| = \left|\hat{\phi}(0)\right| = 1. \tag{65}$$

From (64) we obtain $|H(0)| = 1$. Since the asymptotic decay of $\phi(x)$ at infinity satisfies

$$\left|\phi(x)\right| = O(x^{-2})$$

we can also derive that

$$h(n) = \langle\phi^{-1}(u), \phi(u - n)\rangle = O(n^{-2})$$

at infinity.

Let us now prove property (17b). We saw in Appendix A that a scaling function must satisfy

$$\sum_{k=-\infty}^{+\infty} \left| \hat{\phi}(\omega + 2k\pi) \right|^2 = 1. \qquad (66)$$

Since $H(\omega)$ is 2π periodic, (64) and (66) yield

$$\left| H(\omega) \right|^2 + \left| H((\omega + \pi)) \right|^2 = 1.$$

Let us write

$$\hat{\phi}(\omega) = \prod_{p=1}^{+\infty} H(2^{-p}\omega). \qquad (67)$$

We will show that this equation defines the Fourier transform of a scaling function. We need to prove that

(α) $\hat{\phi}(\omega) \in L^2(\mathbf{R})$ and $(\phi(x - n))_{n \in Z}$ is an orthonormal family.

(β) If V_{2^j} is the vector space generated by the family of functions $(\phi_{2^j}(x - 2^{-j}n))_{n \in Z}$, then the sequence of vector spaces $(V_{2^j})_{j \in Z}$ is a multiresolution approximation of $L^2(\mathbf{R})$.

Let us first prove property (α). With the Parseval theorem, we can show that this statement is equivalent to

$$\forall n \in \mathbf{Z}, \int_{-\infty}^{+\infty} \left| \hat{\phi}(\omega) \right|^2 e^{ik\omega} \, d\omega = \begin{cases} 2\pi & \text{if } k = 0 \\ 0 & \text{if } k \neq 0 \end{cases} \qquad (68)$$

Let us define the sequence of functions $(g_q(\omega))_{q>1}$ such that

$$g_q(\omega) = \begin{cases} \prod_{p=1}^{q} H(2^{-p}\omega) & \text{for } |\omega| < 2^q\pi \\ 0 & \text{for } |\omega| > 2^q\pi. \end{cases} \qquad (69)$$

As q tends to $+\infty$, the sequence $(g_q(\omega))_{q>1}$ converges towards $|\phi(\omega)|^2$ almost everywhere. We can also prove that

$$\forall n \in \mathbf{Z}, \int_{\infty}^{+\infty} g_q(\omega) e^{ik\omega} \, d\omega = \begin{cases} 2\pi & \text{if } k = 0 \\ 0 & \text{if } k \neq 0. \end{cases} \qquad (70)$$

With hypothesis (17c) of Theorem 2, it is then possible to apply the dominated convergence theorem to the sequence $(g_q(\omega))_{q>1}$ to derive from (70) that $\hat{\phi}(\omega)$ satisfies (68).

Let us now prove property (β). In order to prove that $(V_{2^j})_{j \in Z}$ is a multiresolution approximation of $L^2(\mathbf{R})$, we must show that assertions (2)–(8) apply. The properties (2)–(6) can be derived from the equation

$$\hat{\phi}(2\omega) = H(\omega) \hat{\phi}(\omega).$$

Since $H(\omega)$ satisfies (17a), we can show that

$$\left| \hat{\phi}(0) \right| = \left| \int_{-\infty}^{+\infty} \phi(x) \, dx \right| = 1.$$

From this equation, one can prove that the sequence of vector spaces $(V_{2^j})_{j \in Z}$ defined in (β) do satisfy the last two properties (7) and (8) of a multiresolution representation.

APPENDIX D
PROOF OF THEOREM 3

This appendix gives the main steps of the proof of Theorem 3. More details can be found in [28]. This theorem is proved for $j = -1$. We are looking for a function $\psi(x) \in L^2(\mathbf{R})$ such that $(\sqrt{2^{-1}}\psi_2 \cdot (x - 2^{-1}n))_{n \in Z}$ is an orthonormal basis of $O_{2^{-1}}$. The orthogonality of this family can be expressed with the Poisson formula

$$\sum_{k=-\infty}^{+\infty} \left| \hat{\psi}(2\omega + 2k\pi) \right|^2 = 1. \qquad (71)$$

Since $\psi_{2^{-1}}(x) \in O_{2^{-1}} \subset V_1$, we can decompose it on the orthonormal basis $(\phi(x - n))_{n \in Z}$:

$$\psi_{2^{-1}}(x) = \sum_{n=-\infty}^{+\infty} \langle \psi_{2^{-1}}(u), \phi(u - n) \rangle \, \phi(x - n). \qquad (72)$$

Let us define

$$G(\omega) = \sum_{n=-\infty}^{+\infty} \langle \psi_2 \cdot (u), \phi(u - n) \rangle \, e^{-in\omega}. \qquad (73)$$

The Fourier transform of (73) yields

$$\hat{\psi}(2\omega) = G(\omega) \hat{\phi}(\omega). \qquad (74)$$

As in Appendix C, (74) and (71) give

$$\left| G(\omega) \right|^2 + \left| G(\omega + \pi) \right|^2 = 1. \qquad (75)$$

Since $O_{2^{-1}}$ is orthogonal to $V_2 \cdot$, each function of the family $(\sqrt{2^{-1}}\psi_{2^{-1}}(x - 2^{-1}n))_{n \in Z}$ should be orthogonal to each function of the family $(\sqrt{2^{-1}}\phi_{2^{-1}}(x - 2^{-1}n))_{n \in Z}$. The Poisson formula shows that this property is equivalent to

$$\forall n \in \mathbf{Z}, \sum_{n=-\infty}^{+\infty} \phi(2\omega + 2n\pi) \overline{\hat{\psi}(2\omega + 2n\pi)} = 0. \qquad (76)$$

By inserting (64), (66), and (74) in (77), we obtain

$$H(\omega) \overline{G(\omega)} + H(\omega + \pi) \overline{G(\omega + \pi)} = 0. \qquad (77)$$

We can prove that the necessary conditions (75) and (76) on $G(\omega)$ are sufficient to ensure that $(\sqrt{2^{-1}}\psi_{2^{-1}}(x - 2^{-1}n))_{n \in Z}$ is an orthogonal basis of $O_{2^{-1}}$. An example of such function $G(\omega)$ is given by

$$G(\omega) = e^{-i\omega} \overline{H(\omega + \pi)}. \qquad (78)$$

The functions $G(\omega)$ and $H(\omega)$ can be viewed as the transfer functions of a pair of quadrature mirror filters. By taking the inverse Fourier transform of (79), we prove that the impulse responses $(g(n))_{n \in Z}$ and $(h(n))_{n \in Z}$ of these filters are related by

$$g(n) = (-1)^{1-n} h(1 - n). \qquad (79)$$

By definition, a multiresolution approximation of $L^2(\mathbf{R})$ satisfies

$$\lim_{j \to +\infty} V_{2^j} = L^2(\mathbf{R}) \quad \text{and} \quad \lim_{j \to -\infty} V_{2^j} = \{0\}.$$

Since O_{2^j} is the orthogonal complement of V_{2^j} in $V_{2^{j+1}}$, we can derive that that for any $j \neq k$, O_{2^j} is orthogonal to O_{2^k} and

$$L^2(R) = \bigoplus_{j=-\infty}^{+\infty} O_{2^j}. \qquad (80)$$

We proved that for any $j \in Z$, $(\sqrt{2^{-j}}\psi_{2^j}(x - 2^{-j}n))_{n \in Z}$ is an orthonormal basis of O_{2^j}. The family of functions $(\sqrt{2^{-j}}\psi_{2^j}(x - 2^{-j}n))_{(n,j) \in Z^2}$ is therefore an orthonormal basis of $L^2(R)$.

APPENDIX E
PROOF OF THEOREM 4

This appendix gives the main steps of Theorem 4 proof. More details can be found in [35]. Let $(V_{2^j})_{j \in Z}$ be a multiresolution approximation of $L^2(R)$ such that for any $j \in Z$,

$$V_{2^j} = V_{2^j}^1 \otimes V_{2^j}^1 \qquad (81)$$

where $(V_{2^j}^1)_{j \in Z}$ is a multiresolution approximation of $L^2(R)$. We want to prove that the family of functions

$$\left(2^{-j}\phi_{2^j}(x - 2^{-j}n) \psi_{2^j}(y - 2^{-j}m), \right.$$

$$2^{-j}\psi_{2^j}(x - 2^{-j}n) \phi_{2^j}(y - 2^{-j}m),$$

$$\left. 2^{-j}\psi_{2^j}(x - 2^{-j}n) \psi_{2^j}(y - 2^{-j}m) \right)_{(n,m) \in Z^2}$$

is an orthonormal basis O_{2^j}. The vector space O_{2^j} is the orthogonal complement of V_{2^j} in $V_{2^{j+1}}$. Let $O_{2^j}^1$ be the orthogonal complement of $V_{2^j}^1$ in $V_{2^{j+1}}^1$. Equation (81) yields

$$V_{2^{j+1}} = V_{2^{j+1}}^1 \otimes V_{2^{j+1}}^1$$

$$= (O_{2^j}^1 \oplus V_{2^j}^1) \otimes (O_{2^j}^1 \oplus V_{2^j}^1).$$

This can be rewritten

$$V_{2^{j+1}} = (V_{2^j}^1 \otimes V_{2^j}^1) \oplus (V_{2^j}^1 \otimes O_{2^j}^1) \oplus (O_{2^j}^1 \otimes V_{2^j}^1)$$

$$\oplus (O_{2^j}^1 \otimes O_{2^j}^1).$$

The orthogonal complement of V_{2^j} in $V_{2^{j+1}}$ is therefore given by

$$O_{2^j} = (V_{2^j}^1 \otimes O_{2^j}^1) \oplus (O_{2^j}^1 \otimes V_{2^j}^1)$$

$$\oplus (O_{2^j}^1 \otimes O_{2^j}^1). \qquad (82)$$

The family of functions $(\sqrt{2^{-j}}\phi_{2^j}(x - 2^{-j}n))_{j \in Z}$ is an orthonormal basis of $V_{2^j}^1$ and $(\sqrt{2^{-j}}\psi_{2^j}(x - 2^{-j}n))_{j \in Z}$ is an orthonormal basis of $O_{2^j}^1$. Hence, (82) implies that

$$\left(2^{-j}\phi_{2^j}(x - 2^{-j}n) \psi_{2^j}(y - 2^{-j}m), \right.$$

$$2^{-j}\psi_{2^j}(x - 2^{-j}n) \phi_{2^j}(y - 2^{-j}m),$$

$$\left. 2^{-j}\psi_{2^j}(x - 2^{-j}n) \psi_{2^j}(y - 2^{-j}m) \right)_{(n,m) \in Z^2}$$

is an orthonormal basis of O_{2^j}.

The vector space $L^2(R^2)$ can be decomposed as a direct sum of the orthogonal spaces O_{2^j}

$$L^2(R^2) = \bigoplus_{j=-\infty}^{+\infty} O_{2^j}.$$

The family of functions

$$\left(2^{-j}\phi_{2^j}(x - 2^{-j}n) \psi_{2^j}(y - 2^{-j}m), \right.$$

$$2^{-j}\psi_{2^j}(x - 2^{-j}n) \phi_{2^j}(y - 2^{-j}m),$$

$$\left. 2^{-j}\psi_{2^j}(x - 2^{-j}n) \psi_{2^j}(y - 2^{-j}m) \right)_{(n,m) \in Z^3}$$

is therefore an orthonormal basis of $L^2(R^2)$.

REFERENCES

[1] E. Adelson and E. Simoncelli. "Orthogonal pyramid transform for image coding." *Proc. SPIE, Visual Commun. Image Proc.*, 1987.

[2] A. Arneodo, G. Grasseau, and H. Holschneider. "On the wavelet transform of multifractals." Tech. Rep., CPT, CNRS Luminy, Marseilles, France, 1987.

[3] G. Battle. "A block spin construction of ondelettes, Part 1: Lemarie functions." *Commun. Math. Phys.*, vol. 110, pp. 601–615, 1987.

[4] J. Beck, A. Sutter, and R. Ivry. "Spatial frequency channels and perceptual grouping in texture segregation." *Comput. Vision Graph. Image Proc.*, vol. 37, 1987.

[5] P. J. Burt and E. H. Adelson. "The Laplacian pyramid as a compact image code." *IEEE Trans. Commun.*, vol. COM-31, pp. 532–540. Apr. 1983.

[6] F. Campbell and D. Green. "Optical and retina factors affecting visual resolution." *J. Physiol.*, vol. 181, pp. 576–593, 1965.

[7] F. Campbell and J. Kulikowski. "Orientation selectivity of the human visual system." *J. Physiol.*, vol. 197, pp. 437–441, 1966.

[8] J. Crowley. "A representation for visual information." Robotic Inst. Carnegie-Mellon Univ., Tech. Rep. CMU-RI-TR-82-7, 1987.

[9] I. Daubechies. "Orthonormal bases of compactly supported wavelets." *Commun. Pure Appl. Math.*, vol. 41, pp. 909–996. Nov. 1988.

[10] D. Esteban and C. Galand. "Applications of quadrature mirror filters to split band voice coding schemes." *Proc. int. Conf. Acoust., Speech, Signal Processing*, May 1977.

[11] P. Federbush. "Quantum field theory in ninety minutes." *Bull. Amer. Math. Soc.*, 1987.

[12] P. Flandrin. "On the spectrum of fractional Brownian motions." UA 346, CNRS, Lyon, Tech. Rep. ICPI TS-8708, France.

[13] A. Gagalowicz. "Vers un modele de textures." dissertation de docteur d'etat, INRIA, May 1983.

[14] P. Goupillaud, A. Grossmann, and J. Morlet. "Cycle octave and related transform in seismic signal analysis." *Geoexploration*, vol. 23, pp. 85–102. 1985/1984.

[15] N. Graham. "Psychophysics of spatial frequency channels." *Perceptual Organization*, Hilldale, NJ, 1981.

[16] W. Grimson. "Computational experiments with a feature based stereo algorithm." *IEEE Trans. Pattern Anal. Machine Intell.*, vol. PAMI-7, pp. 17–34, Jan. 1985.

[17] A. Grossmann and J. Morlet. "Decomposition of Hardy functions into square integrable wavelets of constant shape." *SIAM J. Math.*, vol. 15, pp. 723–736, 1984.

[18] E. Hall, J. Rouge, and R. Wong. "Hierarchical search for image matching." in *Proc. Conf. Decision Contr.*, 1976, pp. 791–796.

[19] D. Heeger and A. Pentland. "Measurement of fractal dimension using Gabor filters." Tech. Rep. TR 391, SRI AI center.

[20] S. Jaffard and Y. Meyer. "Bases d'ondelettes dans des ouverts de Rn." *J. de Math. Pures Appli.*, 1987.

[21] B. Julesz, "Textons, the elements of texture perception and their interactions," *Nature*, vol. 290, Mar. 1981.

[22] J. Koenderink, "The structure of images," in *Biological Cybernetics*. New York: Springer Verlag, 1984.

[23] R. Kronland-Martinet, J. Morlet, and A. Grossmann, "Analysis of sound patterns through wavelet transform," *Int. J. Pattern Recog. Artificial Intell.*, 1988.

[24] P. G. Lemarie, "Ondelettes a localisation exponentielles," *J. Math. Pures Appl.*, to be published.

[25] P. G. Lemarie and Y. Meyer, "Ondelettes et bases Hilbertiennes," *Revista Matematica Ibero Americana*, vol. 2, 1986.

[26] H. Maitre and B. Faust, "The nonstationary modelization of images: Statistical properties to be verified," Conf. Pattern Recogn., May 1978.

[27] S. Mallat, "A compact multiresolution representation: the wavelet model," in *Proc. IEEE Workshop Comput. Vision*, Miami, FL, Dec. 1987.

[28] ——, "Multiresolution approximation and wavelet orthonormal bases of L2," *Trans. Amer. Math. Soc.*, June 1989.

[29] B. Mandelbrot, *The Fractal Geometry of Nature*. New York: Freeman, 1983.

[30] D. Marr, *Vision*. New York: Freeman, 1982.

[31] D. Marr and T. Poggio, "A theory of human stereo vision," *Proc. Royal Soc. London*, vol. B 204, pp. 301-328, 1979.

[32] J. Max, "Quantizing for minimum distortion," *Trans. IRE Inform. Theory*, vol. 6, pp. 7-14.

[33] Y. Meyer, "Ondelettes et fonctions splines," *Sem. Equations aux Derivees Partielles*, Ecole Polytechnique, Paris, France, Dec. 1986.

[34] ——, *Ondelettes et Operateurs*, Hermann, 1988.

[35] ——, "Principe d'incertitude, bases hilbertiennes et algebres d'operateurs," *Bourbaki seminar*, no. 662, 1985-1986.

[36] Millar and C. Paul, "Recursive quadrature mirror filters; Criteria specification and design method," *IEEE Trans. Acoust., Speech, Signal Processing*, vol. 33, pp. 413 420, Apr. 1985.

[37] A. Papoulis, *Probability, Random Variables, and Stochastic Processes*. New York: McGraw-Hill, 1984.

[38] T. Paul, "Affine coherent states and the radial Schrodinger equation. Radial harmonic oscillator and hydrogen atom," Preprint.

[39] A. Pentland, "Fractal based description of natural scenes," *IEEE Trans. Pattern Anal. Machine Intell.*, vol. PAMI-6, pp. 661-674, 1984.

[40] G. Pirani and V. Zingarelli, "Analytical formula for design of quadrature mirror filters," *IEEE Trans. Acoust., Speech, Signal Processing*, vol. ASSP-32, pp. 645-648, June 1984.

[41] A. Rosenfeld and M. Thurston, "Edge and curve detection for visual scene analysis," *IEEE Trans. Comput.*, vol. C-20, 1971.

[42] ——, "Coarse-fine template matching," *IEEE Trans. Syst., Man, Cybern.*, vol. SMC-7, pp. 104-107, 1977.

[43] A. Watson, "Efficiency of a model human image code," *J. Opt. Soc. Amer.*, vol. 4, pp. 2401-2417, Dec. 1987.

[44] J. W. Woods and S. D. O'Neil, "Subband coding of images," *IEEE Trans. Acoust., Speech, Signal Processing*, vol. ASSP-34, Oct. 1986.

Stephane G. Mallat was born in Paris, France. He graduated from Ecole Polytechnique, Paris, in 1984 and from Ecole Nationale Superieure des Telecommunications, Paris, in 1985. He received the Ph.D. degree in electrical engineering from the University of Pennsylvania, Philadelphia, PA, in 1988.

Since September 1988, he has been an Assistant Professor in the Department of Computer Science of the Courant Institute of Mathematical Sciences, New York University, New York, NY. His research interests include computer vision, signal processing, and applied mathematics.